Twenty-Third Symposium on Naval Hydrodynamics (2001)
Naval Studies Board (NSB)

Breaking Waves in the Ocean and around Ships

M. P. Tulin [1] and M. Landrini [2]

[1] *Ocean Engineering Laboratory*, UCSB, mpt@engineering.ucsb.edu
[2] INSEAN, *The Italian Ship Model Basin*, Italy, maulan@waves.insean.it

ABSTRACT

A wide ranging summary of research on ocean and ship breaking waves carried out within the Ocean Engineering Laboratory at the University of California, Santa Barbara, beginning in 1985, is presented in a coherent fashion. Emphasis is given to the role of naturally arising wave modulations in their crucial effect on wave breaking, as well as on the essential role which wave breaking plays in wave evolution. The OEL criterion for the onset of wave deformation and breaking is discussed and its mathematical derivation is given; its experimental validation through surface orbital velocity measurements is reviewed. The recent development of a gridless numerical simulation method for the study of post breaking wave flows is discussed, and examples of splashing flows are given, including bores, and bow breaking waves produced by a Wigley hull. Comparison with laboratory and field observations are made whenever possible.

1 FORWARD

In 1985 we began our studies of breaking waves at the newly founded Ocean Engineering Laboratory within the University of California at Santa Barbara. We began with Raymond Cointe's analysis of the steady breaker above a submerged hydrofoil, Cointe and Tulin (1994), where good experimental data existed, Duncan (1983), and for which we obtained some predictions of breaking and breaker characteristics, based on a breaker model consisting of an essentially stagnant eddy, Figure 1, riding on the forward face of the leading wave in the wave train behind the hydrofoil and held in place by shear stresses along the dividing streamline. This model was quantified utilizing independent measurements of the turbulent shear stresses, and it was shown that the hydrostatic pressure acting on the dividing streamline underneath the eddy creates a trailing wave which largely cancels that trailing wave which would exist in the absence of breaking. The 'wave' resistance of the hydrofoil thus manifests itself in the momentum flux of the residual trailing wave plus the breaker resistance, *i.e.* the momentum flux in the breaker wake. The total resistance for a fixed hydrofoil speed was shown to have a minimum corresponding to a particular value of the trailing wave steepness resulting in an onset condition for breaking.

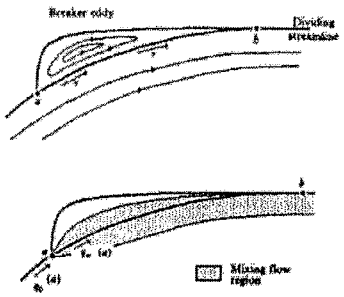

Figure 1: Physical model of a quasi-steady spilling breaker.

In contrast to the quasi-steady hydrofoil breaker, energetic waves in the ocean are transient by their nature, and subsequently we have sought to gain a fundamental understanding of the latter, and of their effect on the nonlinear dynamics of ocean wave evolution. We early concluded, Li and Tulin (1992), that energetic breaking was closely associated with these nonlinear dynamics, especially wave modulation (groups) caused by instability of the Benjamin-Feir type. As time went on we utilized various methods, as necessary, including analysis, exact numerical simulations, and a variety of experiments in our small and large wind wave tanks, Figure 2, including the use of radar.

In response to needs of the Navy, we also

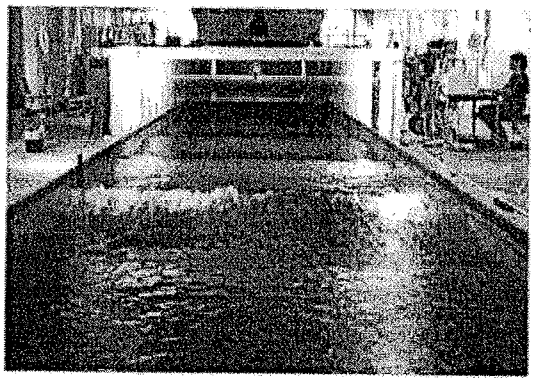

Figure 2: The large OEL Wind-Wave Tank.

turned our attention to those breaking ship waves produced by the bow and which contributed to the pervasive surface wakes seen behind ships. For these studies we have relied heavily on nonlinear $2D + t$ numerical simulations, and these have been recently extended to the post-breaking regime dominated by surface turnover and splashing.

It now seems time to present a wide-ranging summary of the various results which have been obtained. This is done first through an extended Overview, followed by two separate sections with more detail; Section 3 is devoted to the mechanism of breaking, and Section 4 to the numerical treatment of wave splashing and to splashing bow waves on ships and their near wake.

We are concerned here with an exposition of our own work, and this should therefore not be construed as another attempt to review the widespread literature. For that there exist several recent reviews, Longuet-Higgins (1996) and Melville (1996). The first of these gives particular emphasis to theoretical work on the stability of steep waves, and the second to experimental and field observations.

A large number of talented individuals connected with the OEL have taken part in the investigations which led to the present results, and this paper is fondly and gratefully dedicated to all of them, who have taught me so much. Their names will be found as authors of the OEL related papers in the References. During the last few years we have much benefited from a close working collaboration with my co-author, Maurizio Landrini, of INSEAN, Roma, who is now in charge of our numerical simulations of breaking and post breaking ship waves. He has written Section 4.

The investigations reported on here were all supported by the Office of Naval Research, the investigations of ocean-like breakers by the Ocean Technology Division under a sequence of Program Officers (Gene Silva, Steve Ramberg, and Tom Swean *jr.*), and the investigations of ship breakers first by Jim Fein, and then by the Ship Hydrodynamics Program under Ed Rood. Their faithful support of the OEL from its first beginnings until the present time has been absolutely crucial to its development and its productivity, and we cannot thank them enough.

2 OVERVIEW

2.1 1985

Our own view of both ocean and ship breakers has been radically transformed since we began our studies of breaking in 1985.

The description of ocean waves was then, as it largely remains now, stochastic in nature, and the prototype wave was considered synonymous with the Stokes wave. Prevailing notions then related the breaking of energetic waves to the Stokes Limiting Wave, either through the Longuet-Higgins (1969, 1977, 1985) crest acceleration criterion, or through a wave steepness criterion determined experimentally; the Phillips energy spectrum, for ocean waves, which had enjoyed wide popularity, was entirely based on the notion that the saturated (breaking) wave at every scale shared the same geometry, depending only on g, as in the case of Stokes waves.

Theorists had by then suggested that wave modulations of nonlinear origin might be crucial for ocean modeling, Yuen and Lake (1982); field observations of waves breaking at the peak of wave groups had been made, and systematic and insightful laboratory experiments on a large scale were being carried out. However, the significance of modulations for the breaking of waves, whether due to natural instability (group formation) or to wave-wave interactions, had not been well appreciated or understood. In fact, a small minority of the publishing wave community even accepted the existence of wave groups in the ocean, notable among them Su (1986), and Goda (1976).

By 1985, a large body of literature existed on nonlinear wave interactions, originating in the pioneering work of Phillips (1960), on the four wave interaction mechanism, and in the form of the kinetic theory of waves by Hasselman (1962) and Zakharov (1968), and their new ideas were widely accepted within the theoretical ocean community and even incorporated into wave forecasting methods, Swamp Group (1985). In these kinetic equations the effect of breaking and wind pumping on the wave dynamics has been ignored. The reason has been given that these real processes are slower than wave interactions and therefore noncompetitive. In wave forecasting this neglect would be fatal and therefore wave energy (or wave action) evolution is driven by wind pumping suitably reduced by energy dissipation due to breaking, all suitably parameterized in terms of the wave energy. Wave momentum considerations are neglected throughout, and this creates a vacuum regarding the evolution of wave frequency, a vacuum which is filled with certain largely empirical results from wave interaction calculations. This unsatisfactory situation continues, in fact, until the present time, although the effects of breaking on wave dynamics, particularly frequency downshifting, has been elucidated through experiments, Tulin and Waseda (1999), and theory, Tulin (1996).

In 1985, the situation regarding the divergent bow waves from ships, and their breaking was underdeveloped and unsatisfactory. The only coherent view of these waves was as a part of the traditional Kelvin wave pattern, represented by the divergent portion of the ship's wave amplitude spectrum. The use of the Neumann-Kelvin method for the prediction of wave resistance continued this spectral representation of the divergent waves in that it incorporated the Havelock singularity based on linear considerations, as had the Michell theory and its slender body representation. Disquiet was injected into this situation by the experimental studies in Tokyo, Inui *et al.*(1979), and Miyata, (1980), which showed the appearance of a single almost straight wave crest at the bow, whose angle of inclination depended on the ship speed. Neither of these observed characteristics were understandable in terms of conventional theory, and it remained for nonlinear simulations, based on the $2D + t$ approximations, much later to reproduce and explain these results, Tulin and Wu (1996).

The splashing, mixing, air entrainment, and noise generation which occurred in the aftermath of breaking of both energetic ocean waves and divergent bow waves, and are of such great interest today, had been seldom studied, with the exception of the hydraulic jump, or bore, about which a little was known. Our state of ignorance was nowhere more critically revealed and our curiosity prodded than by the stimulating reviews of Peregrine (1981), Melville (1996), the experiments of Bonmarin (1989), and our own experimental observations. Our own understanding of both ocean and ship breaking waves has been achieved in good part because of our high resolution simulation methods, LONGTANK and $2D+t$, both based on boundary elements, and it was natural for us to extend simulations into the regime of splashing. This has required the use of a gridless Euler solver, based on a Smoothed Par-

Twenty-Third Symposium on Naval Hydrodynamics (2001)
Naval Studies Board (NSB)

Web Search Builder
Skim This Chapter
Reference Finder

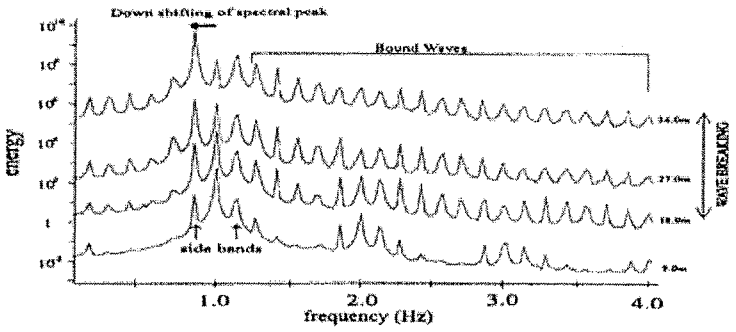

Figure 3: Wave energy density spectra at various fetches (9-36 m) from the wavemaker, measured with wave wires in the large OEL Wind Wave Tank. The evolution of the instability until breaking and subsequent downshifting is demonstrated.

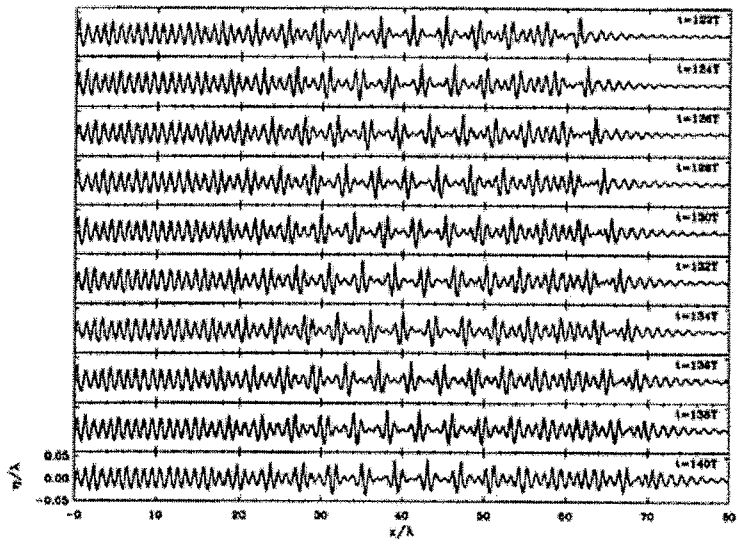

Figure 4: Modulating waveforms in space, created by a wavemaker at the far left, for a sequence of times. The growth of the instability, wave group formation, and partial recurrence can be seen. LONGTANK simulation.

ticle Hydrodynamics Lagrangian technique and which we call *SPlashH*.

2.2 Wave Modulation

The instability growth and modulation of a nearly monochromatic wave has been demonstrated both in the laboratory, Lake *et al.* (1977), Melville (1982), Su and Green (1985) and Tulin and Waseda (1994), and in numerical simulations, Wang *et al.* (1994), and the connection with breaking has been conclusively demonstrated.

The evolution of a wave system through modulation, breaking, and downshifting is seen through the measured spectra taken in the OEL wave tank (175'L×14'W×8'D), Figure 3. A time-distance simulation of a similar wave system, using the OEL numerical wave tank, LONGTANK, is shown in Figure 4.

In the Ocean Engineering Laboratory (OEL) at UCSB we regularly produce waves breaking in self-excited wave groups for the purpose of studying the radar back scatter from a low grazing angle coherent radar.

We have also used wave groups in the OEL tank to study the loadings on floating bridge structures, Welch *et al.* (1996), and to study the response of flexible vertical cylindrical structures to excitation in deformed and breaking waves, Welch *et al.* (1999).

Do such wave group modulations occur in the ocean, and do they cause wave breaking? The evidence is that they do. The earliest observations and connections between ocean wave groups and breaking include: Donelan *et al.* (1972), Rye (1974), Goda (1976), Su *et al.* (1982) and Holthuijsen and Herbers (1986). Despite these, there has been much controversy amongst ocean engineers, where the concept of a stochastic sea has proven so useful and has therefore become deeply imbedded. Most of all, the visualization and measurement of wave groups has not been clear-cut, and a clear overall picture of how they exist in the ocean and under which conditions has not yet been obtained.

Recently, however, low grazing angle (6°) coherent radars when viewing wind waves in the field, have produced remarkable range-time $R-t$ maps which unmistakably show the existence of wave groups, Werle (1995), Smith and Poulter (1993), Ivanov (1993). Figure 5 is an actual radar image together with an explanatory sketch. These maps show bursts of scattering along straight lines in the $R-t$ diagram and the analysis of these shows that the slope of the lines conforms to the law $c_g = dR/dt$ and the temporal spacing of the bursts is $2T$. A large number of these maps have been obtained in sheltered waters, but they have been seen in the open ocean (Ivanov) and more experiments are underway.

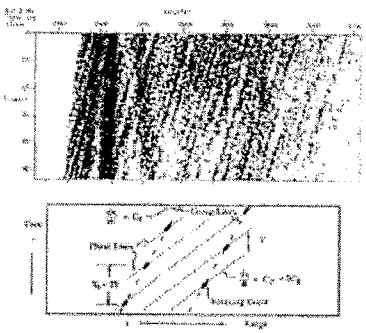

Figure 5: Top: range-time radar return from a low grazing angle, coherent radar mounted on a cliff overlooking Lock Linnhe; the bursts are breaking events. Bottom: a range-time schematic allowing a quantitative analysis of the upper figure.

There is of course a theoretical basis for these nonlinear wave groups. In the first place, it had been shown long ago by Benjamin and Feir (1967) that monochromatic waves are unstable to small sidebands, although the theory does not allow for spatial variations in the wave system, only temporal. The space-time evolution of the resulting wave train was later studied, both theoretically and experimentally by Lake *et al.* (1977); they employed the weakly nonlinear model (the nonlinear cubic Schrodinger equation, NLS) first introduced by Benny and Newell (1967).

Later, exact nonlinear simulations showing wave group modulations were first carried out by Dold and Peregrine (1986), and subsequently a technique was developed at the OEL for simulations of very long wave trains, specifically for the purpose of understanding breaking in wave groups. These allowed long time exact inviscid studies of wave instability growth, wave

group formation, and wave breaking, see Wang *et al.* (1994).

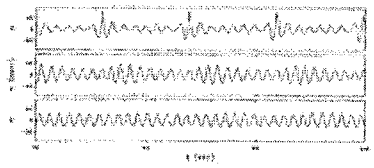

Figure 6: Temporal wave records in the large OEL Wind Wave Tank. Fetches from the wavemaker: 27 m (upper); 18 m (middle); 5 m (lower). Strong grouping and breaking (upper), and energy concentration under the group peak.

What are the possible effects of wave group modulations? Most important, wave energy becomes concentrated under the peak of the envelope, and this effect is strongest near breaking as shown in Figure 6, a wave elevation time series taken in the OEL tank of modulating wave groups near breaking. A summary of available information on this concentration effect of grouping is shown in Figure 7, where data on the relation between $H_{max_0}/2$ and the wave steepness before modulation, a_0k_0, are shown, based on laboratory measurements, Su and Green (1985), and simulations, Wang *et al.* (1994). Under realistic conditions ($ka \simeq 0{\cdot}12$), the wave height at the peak of the envelope is seen to be almost double its initial value. This alone, points up the potential importance of wave groups for us. Connected with this fact, there is ample evidence connecting breaking with wave groups, and it is during breaking that heightened crests and steepened wave faces occur. We discuss these subsequently.

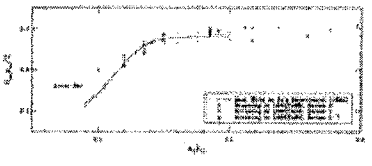

Figure 7: The wave height at breaking $H_b k_0/2$ *vs.* the initial wave steepness a_0k_0, from tank experiments, Su and Green (1985), and simulations by LONGTANK.

2.3 Wave Deformation

Surface wave kinematics approaching breaking and during the breaking process change dramatically from those we expect based on quasi-sinusoidal wave forms. First of all, the almost circular motion of individual surface particles becomes disrupted, resulting in a much larger down-wave drift than Stokes, which varies as $(ak)^2$. This effect, in fact, occurs before breaking according to LONGTANK simulations, see some examples in Figure 8. Then, as the face progressively steepens in time, see Figure 9, the motion of a large part of it becomes directed toward the normal to the surface, and the particles are accelerated down tank, see Figure 10.

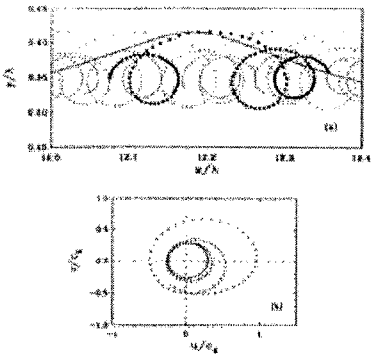

Figure 8: Top: Particle trajectories, non-breaking modulating wave, LONGTANK. The dots are separated by constant intervals in time. Note occasional large excursions, when group peaks have passed by. Bottom: Horizontal, u, *vs.* vertical , v, velocity for a particle, which eventually made a large excursion.

As a result of both increase in H and the rise of the crest, the amplitude of the crest is much increased, see Figure 9. Of course, this crest rise is very important in the estimation of platform requirements. A crest rise factor, A_{max}/H, in the range 0·74 to 0·80 has been found in LONGTANK simulations. This is larger than the value of 0·6 suggested for engineering applications, Stansberg (1991), but close to the value 0·77 quoted by Kjeldsen (1990) for breaking waves in his tank experiments.

These deforming waves found in LONGTANK simulations have also been observed in tank measure-

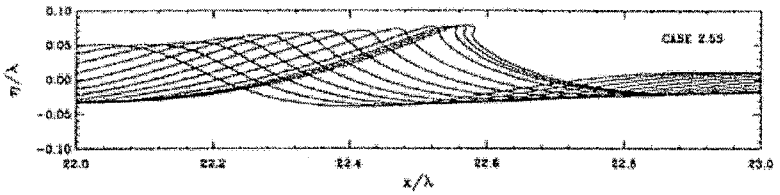

Figure 9: Wave Deformation from Inception (left) until Jet Formation (right), LONGTANK.

ments at the OEL. A set of wave profiles measured with a 1d wire linear array in the large UCSB wave tank is shown in Figure 11 compared with a simulation; the wave length is 2·3 m and the modulating waves were measured at about 100' from the wavemaker.

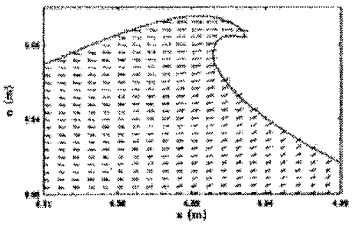

Figure 10: The velocity field within a breaking wave with jet, LONGTANK.

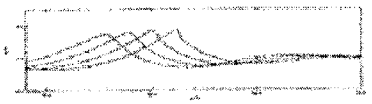

Figure 11: A comparison of breaking wave profiles measured in the large OEL wind-wave tank (dots) with LONGTANK simulations (lines).

The connection between asymmetric deformation (front face steepening) and the breaking of extreme waves at sea was first made by Kjeldsen and Myrhaug (1980), based on observations. They claimed that extreme waves are accompanied by a shallow trough and a steepened wave face; they defined a deformation parameter, see Figure 12, and a critical minimum value for breaking. The LONGTANK simulation of wave breaking in wave groups and the OEL measurements clearly confirm the K-M ocean observations, and partially confirm the value of their deformation parameter see Wang *et al.* (1994); in the light of the breaking criterion found in LONGTANK, the deformation has to be viewed as a consequence of the breaking process and not the cause of it; and the K-M deformation parameter serves to quantify the deformation just before jet formation, and not as a criterion for breaking.

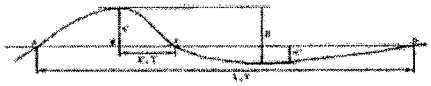

Figure 12: Extreme wave, deformation sketch after Kjeldsen and Myrhaug (1980). For breaking: $[\eta'/H][\lambda/\lambda'] > 3{\cdot}5(K - M)$, and 3·48 – 5·29 (LONGTANK)

2.4 Inception and Mechanism of Breaking

We now have a clear understanding of the exceptional role played by wave modulation in the initiation of wave deformation and breaking, and furthermore we possess a simple criterion for the initiation of this process as the wave passes through the modulation peak. In Section 3 of this paper we present theory which explains the mechanism associated with this criterion, and also its experimental verification through surface particle tracking experiments.

As we have noted, wave modulation in the ocean is a result of wave instability of the Benjamin-Feir type, and this newly described mechanism leads to breaking at group-averaged steepnesses as low as about 0·1. This explains those field observation, Holthuijsen and Herbers (1986), Weissman *et al.* (1984), which came to our attention at the beginning of our work, and

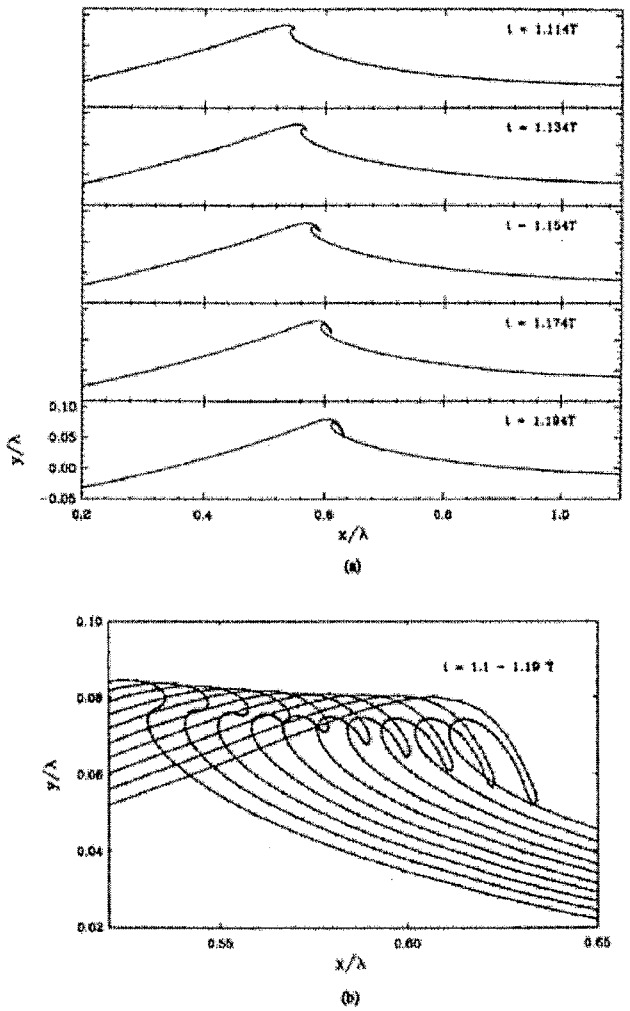

Figure 13: Wave breaking in LONGTANK, $a_0 k_0 = 0.28$. (a): waveforms in the initial stage of breaking. (b): the formation of a plunging jet.

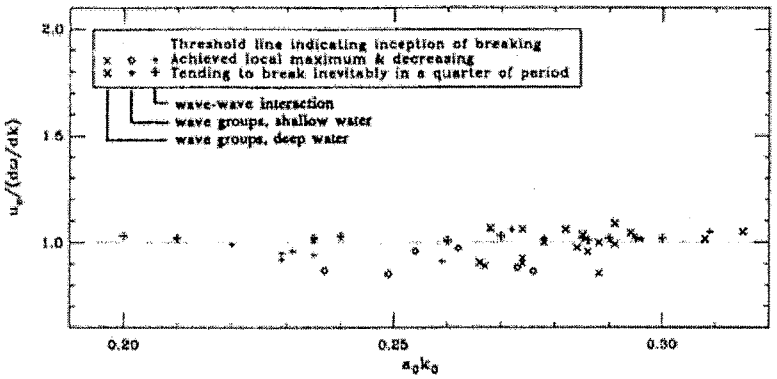

Figure 14: The ratio (crest particle velocity)/(wave group velocity), u_c/c_g, vs. a_0k_0. The horizontal line demarcates waves which did not proceed to breaking from those which did. The value of u_c is determined just prior to wave deformation and jet formation in the case of the breaking waves.

for which no explanation could be found in either laboratory derived breaking measurements, Ochi and Tsai (1983); Ramberg and Griffin (1987), or in prevailing theory, Longuet-Higgins (1969, etc.). These aforementioned field measurements of wave breaking at relatively low values of wave energy, together with field observations of wave breaking in wave groups, Donelan *et al.* (1972), and the field observations and classification of wave deformation associated with large waves, Kjeldsen and Myrhaug (1980), all provided those clues which we can easily read today. Indeed, the observation of breaking in wave groups has first led us in the late 1980's to emphasize the phenomena of wave instability and group formation. Analytical studies of these processes, Tulin and Li (1992), convinced us that the actual process of wave deformation and breaking were probably inaccessible to treatment via the usual weakly nonlinear approaches, perturbation expansion theory for instance. This led us to the development of the high resolution numerical wave tank, LONGTANK, and to numerical experiments of wave group formation leading to breaking, wave deformation and of the inevitable formation of the jet and of its growth and descent in a ballistic trajectory, Figure 13. Most remarkably, a simple criterion for the initiation of deformation was found from the LONGTANK studies:

"that upon passing through the peak of a modulation group, when the orbital velocity at the wave crest, u_c, exceeds the wave group velocity $d\omega/dk = c_g$, then the wave crest and trough both rise, the front face steepens, the wave crest sharpens, and eventually a jet forms at the crest, leading finally to splashing and a breakdown of the wave."

This criterion was found to apply not only for deep water waves where $d\omega/dk \approx c/2$ where c is the wave celerity, but for modulating waves in shallow water too, where $d\omega/dk$ is significantly smaller, Figure 14. In the comparisons shown there, the Stokes second-order dispersion relation was used to calculate c_g.

Theoretical understanding has been elusive, but we have finally succeeded in demonstrating that the usual almost sinusoidal motion of propagating waves fails for modulating waves when in deep water the aforementioned criterion, $u_c = c_g$, is reached.

Recently we have measured the orbital velocity of waves in the presence of mechanically generated wave groups, and confirmed this criterion experimentally as described in Section 3.

2.5 The Effects of Breaking on Wave Evolution

We know now that the application of wave theories toward understanding of real ocean waves requires the introduction of real effects like wind pumping and dissi-

pation. After all, the waves only exist because of the wind, and the most systematic measurements of wave growth (fetch limited growth) reveal a scaling of the fetch laws with the wind speed. We know, too, that for moderate to equilibrium wave systems the breaking dissipation is of the same order as the wind pumping.

We have ourselves tried to understand and quantify the role of real effects in the dynamic evolution of waves. Our first attempts, described in (A) below involved the use of the modified complex evolution equation (NLS), where we have introduced the breaking dissipation as a right-hand forcing term, as others before us, Trulsen and Dysthe (1990); Hara and Mei (1991). Unlike most previous work, however, we have introduced a dissipation dependent upon $(ka)^8$; we had discovered that only for this particular power law dependency on steepness would the breaking dissipation balance the wind input for waves in equilibrium, provided that Toba's law of individual waves is invoked. Later we have confirmed that this law is consistent with the observed fetch laws.

In the mid 90's we have realized the great importance of momentum considerations in addition to energy. In particular, we discovered that the dual conservation laws for energy and momentum can be combined to produce a law for wave speed evolution, and can quantify downshifting, Tulin (1996). This is briefly described in (B) below.

(A) The NLS allows the calculation of possible shapes of the equilibrium modulational envelope; however, without consideration of wind pumping and dissipation, the envelope of groups which actually arise in nature cannot be predicted. Therefore, Li and Tulin (1993), used this model equation including real effects to predict envelope shapes in general. A major result of this study was a prediction of the number of waves in a spatial group as a function of the ratio of maximum and minimum wave steepness, in the group. For values of this ratio between about 0.3 and 0.08, the number of waves varies between about 2 and 7. These results are consistent with the observations of Holthuijsen and Herbers (1986). Note that the number of waves in the temporal group would be twice the quoted numbers. Later, Li and Tulin (1994) thoroughly considered the long time evolution of sideband systems with wind and dissipation, using their modified NLS and dynamic systems analysis; they discussed the strange attractors and possibilities of chaotic behavior.

(B) As breaking proceeds, water flows into the plunging jet, carrying with it, both kinetic and potential energy E and momentum q. Upon splashing, these are lost to the organized wave motion and these losses must be accounted for in the further evolution of the wave. This requires conservation laws for both wave energy and momentum, which may be constructed on the basis of weak non-linearity. We have first done this on a heuristic basis, Tulin (1996), and furthermore shown that a set of evolution equations for E-c correspond to the original, E-q pair. More recently we have derived these same conservation laws from variational considerations including a rigorous inclusion of breaking in the variational formulation; this was done by introducing, in addition to the usual wave Lagrangian, a work function representing the effect of breaking and wind input on the flow dynamics, and by a rigorous definition of this function, Tulin and Li (1999). In addition, we have shown that our set of conservation laws for energy and wave speed can be combined into the complex Landau-Ginzberg or NLS equation, giving the latter new meaning, and extending it to include the effect of breaking in a rigorous way. Here is the newly modified NLS, valid for all (X,T):

$$A_T + c_g A_X + i(c_g/4k)A_{XX} + i\omega k^2|A|^2 A = A\left[\frac{\dot{c}_{\omega_c} - D_k}{g|A|^2} - i4\gamma\int\frac{kD_k}{g|A|^2}dX\right] \quad (1)$$

where (X,T) are the long time and space scales, $A = ae^{i\theta}$, where θ is the wave phase, $\dot{c}_{\omega_c}$ and D_k are the rate of the wind pumping and breaking dissipation, respectively; $\dot{c}_{\omega_c} \sim g|A|^2$, $D_k \sim g|A|^4$ where the constants of proportionality follow from the field observations; $\gamma = O(1) > 0$.

A consequence of the law for the wave celerity is that breaking leads to a continual increase in the wave speed (frequency downshifting) at a rate controlled by the breaking process. The way in which this works was studied in our large wind-wave tank through laboratory observations of wave group evolution, including breaking effects, Tulin and Waseda (1999). A crucial aspect is the cooperation of breaking dissipation and momentum loss acting together with near-neighbor energy transfer in the discretized spectrum, this transfer being due to detuned resonance acting over a limited time (less than 50 wave periods). This is a very different point of view than is commonly incorporated in large-scale wave prediction modeling, where the conservation of wave momentum is ignored.

2.6 On the Modeling of Splashing, and its Consequences

We are indebted to the early, careful, experimental observations of Bonmarin (1989) for some knowledge of the splashing process, which follows wave breaking. These depended heavily on photographic visualization. Recently we have undertaken detailed studies of the entire splashing process and its mechanics, making use of a high-resolution numerical simulation, *SPlasH*. This is described in Section 4. The simulations reveal the presence of the partial forward ricochet of the plunging jet, the collapse of the cavity under the jet, and a backward counter-jet created in reaction, and of the eventual formation of a dipole structure with downward momentum behind the splashing breaker. These all seem consistent with Bonmarin's observations. We have systematically studied the special case of the propagating bore in shallow water, as this has been much studied in the past, and therefore offers an opportunity for validation of the simulation. We have found the simulated propagation of the bore in excellent agreement with predictions based on mass and momentum conservation. The simulation method allows for arbitrary variations in the fluid density, and we intend to extend the present simulations to include the presence of entrained air in the large scale flow structures and to the eventual fate of this air.

2.7 Surface Tension Effects; Microbreakers

The local curvatures in the wave geometry are largest at the crest of a deformed wave in its later pre-jet stage and in the jet itself, whose thickness may only be a few percent of the wave amplitude. We have carried out LONGTANK simulations of modulating and breaking waves, including the effect of surface tension, for waves of varying length down to 25 cm. Scaling shows that the effect of surface tension increases with reduction in the length of the wave. For those waves, simulations showed that surface tension does not effect the breaking criterion and has insignificant effect on the wave deformation except in reducing somewhat the largest curvatures at the crest of the wave prior to breaking. Surface tension (or the length scale) does, however, have a pronounced effect on the jetting process for waves shorter than about 2 m in length. For 1 m waves the jet is considerably rounded and weakened, which explains both visual and radar observations of breaking waves in the OEL large wind-wave tank, where much less energetic splashing is observed for waves 1 m and shorter. For waves between about 25 and 75 cm the jet does not appear at all, to be replaced by a forward facing bulge growing out of the wave crest, Figure 15.

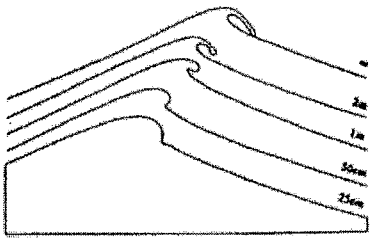

Figure 15: The effect of surface tension on the jet development. Wave profiles were computed with LONGTANK. Microbreakers have wavelength below 1m and surface tension reduces the jet to a bulge.

Non-jetting waves of this kind have been called micro-breakers. Unlike energetic breakers where the shape continually evolves in transient fashion, continually changing over a time interval of about one wave period, the microbreaker can propagate for a considerable distance without significant change of shape. This can be seen in radar tracks in range-time diagrams, since the bulges on the microbreaker crests provide a relatively strong specular radar return, Fuchs and Tulin (2000), Figure 16. A striking feature of the microbreaker bulge is the appearance at the foot of the bulge of a small region of very high curvature, see Figure 15. It is well known that vorticity is generated at a free surface with curvature, and there is ample evidence, Duncan (1994, 1996), Dommermuth and Mui (1996), that a strong effect of this kind does originate at the foot of the bulge, causing dissipation and probably resulting eventually, for very short waves (sub-microbreakers), in the separation of the bulge from the main wave flow through a strong shear layer, forming a cap on top of the wave, as noted by Ebuchi *et al.* (1987). This small scale flow then bears a family relation to the steady hydrofoil breaker, Figure 1, differing in its more or less symmetric placement over the wave crest. Ebuchi and Toba's waves were wind generated, and it may very well be that the wind stress plays an important role in allowing the propagation of this unusual wave.

The microbreaker itself is the consequence of

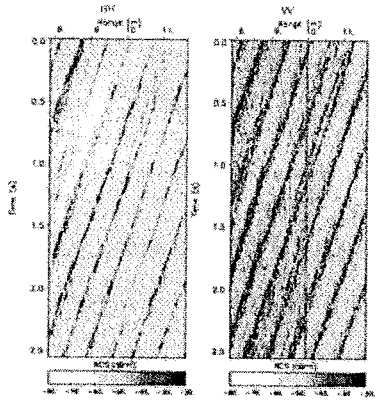

Figure 16: Range-Time-Intensity diagrams of 75 cm wind waves moving toward the ultra high resolution radar at zero range. Each trace originates from compact scattering at the bulge on the crest of each individual microbreaker.

the growth of shorter waves due to the action of wind. As we have observed in our large wind-wave tank, the growth of these waves is very much effected by the existence of breaking energetic waves, which not only modulate the microbreakers, but virtually eliminate them as the microbreaker train is overcome by the energetic breaker at the peak of the wave group. It would seem, observing this striking phenomenon, that it is the action of the energetic breakers which causes the microbreakers to disappear, and that they then begin growing again from very short waves. Their eventual length is thus determined by the effective fetch between energetic breakers.

3 WHEN AND WHY DO MODULATED GRAVITY WAVES BREAK?

3.1 The breaking process, and criterion

Questions of stability aside, Stokes waves in water of constant depth exist for height to length ratios, H/λ, up to a limiting value where the orbital velocity at the crest of the wave, u_c, becomes equal to the wave celerity, c, whereupon the limiting wave crest becomes pointed with an included angle of 120°. Although these facts are presented and highlighted in almost every book on hydrodynamics which discusses waves, it is to our knowledge left unsaid whether waves with steepness as large as the Stokes limiting value have, in fact, been observed experimentally. Undeniably such experiments face difficulties, not only due to wave maker effects, to wall and bottom viscous dissipation and momentum loss, to surface tension modifications, but finally to side-band destabilization of the wave in water of sufficient depth. As is well known, the consequence of this destabilization is for the amplitude of deep water waves to modulate, with the result that the Stokes waves are not only modified but their steepness varies widely over different parts of the wave train.

That these effects occur in nature, too, and invalidate the simple Stokes model has not been sufficiently appreciated. Over the last ten years, however, the process of the breaking of progressive planar waves has been described both in new detail and in a new light. In particular, fully nonlinear and high resolution simulations of a destabilized, monochromatic Stokes wave, carried out in the numerical wave tank, LONGTANK, Wang *et al.* (1994); Wang *et al.* (1995); Yao *et al.* (1994); Tulin *et al.* (1994), have led to a description of breaking with the following features:

- inception as the wave passes through the peak of a modulation,
- an irreversible wave deformation in which the crest and trough both rise, and the front face steepens,
- an increase in the orbital velocity at the crest,
- the emergence of a jet at the crest,
- growth of the jet and descent in a ballistic trajectory,
- splashing.

The way in which this highly transient process evolves in time is indicated in Figure 17, which is based on both simulations and experimental observations.

Remarkably, it was discovered by Dr. Y. T. Yao, from detailed study of the LONGTANK simulations of modulating waves that a well defined criterion exists for the onset of the initial wave deformation in both deep and shallow water: $u_c \approx c_g$, where u_c is the horizontal orbital velocity at the wave crest.

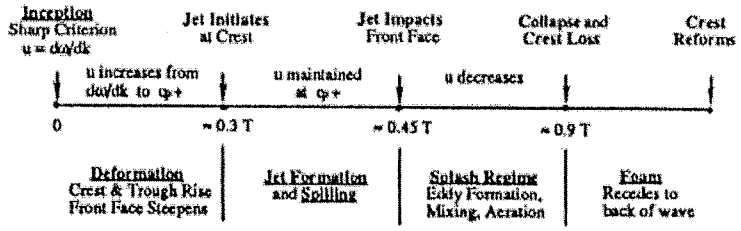

Figure 17: Phases in the wave breaking process.

and c_g is the estimated group velocity of the wave. This criterion was also found to apply for short waves being swept by longer waves, Figure 14.

We have hesitated to publish this criterion in an archival journal, without further confirmation. The result has nevertheless become known, but has not elicited comment in print, except for the skeptical remark, Longuet-Higgins (1996), that it does not work for a shallow water soliton. We had probably not sufficiently emphasized the importance of modulations in the breaking process, since the soliton is not a modulating wave. In fact, for sufficiently long waves in shallow water, sideband instability no longer exists, and the modulations, if they exist, must have been present in the wave trains as they proceed into shallow water. Then, of course, the surf zone or submerged bars provide other mechanisms for breaking. Here we present both some analytical understanding of this inception condition, and in addition, experimental confirmation. The experiments involved automated video measurements of the orbital surface velocities in modulated waves, Matsiev *et al.* (2000).

3.2 Theory of the breaking criterion.

Considering the striking simplicity of the criterion, we believed that its proof by mathematical means would be a simple matter. Nevertheless our search for the proof of the criterion went on unsuccessfully, part time, until recently. Interestingly enough, the search produced its own separate by-products, particularly a study of the detailed process of energy transport in surface waves, Tulin (1997), which led to new insights about the actual meaning of the group velocity.

Eventually we were led to understand that the progressive and sinusoidal shape characteristic of wave motion and which underlies the entire Stokes development, as well as its extension to modulating waves, should not be taken for granted. The strongest empirical evidence for this is the behavior of the wave itself during the breaking process- first, the deformation of the wave into a clearly non-sinusoidal shape, and finally its breakdown through jet overturning and splashing.

The mathematical demonstration of this failure of progressive wave motion reveals that the modulated sinusoidal progressive wave is incompatible with kinematical requirements while passing through the peak of a modulation once $u_c > c_g$.

The demonstration of this incompatibility involves a calculation of the rate of change of the direction, α, of the crest particle velocity vector $qe^{i\alpha}$, as the crest, M, passes through the peak of the wave group, N. For a progressive wave of stationary form, the Stokes wave for example, the trajectory of the crest is a horizontal line, so that $d\alpha/dt|_M = \dot{\alpha}_M = 0$. However, in the case where the crest passes through the peak of the concave modulation envelope and must therefore decelerate, it is necessary that

$$\dot{\alpha}|_{M,N} < 0 \,. \qquad (2)$$

It is not difficult to show that this is not possible for gravity waves in water of any depth, when $u_c > c_g$. In general,

$$\log q - i\alpha = \log(u - iv) \,, \qquad (3)$$

from which it follows that

$$q^2 \frac{d\alpha}{dt} = -u\frac{dv}{dt} + v\frac{du}{dt} \,, \qquad (4)$$

where (u, v) are the (x, y) components of the velocity vector.

At M,N, the vertical component $v \equiv 0$, and

Search This Book GO
Page 725

therefore

$$u_c \left.\frac{d\alpha}{dt}\right|_{M,S} = -\left.\frac{dv}{dt}\right|_{M,S}, \tag{5}$$

where

$$v = \frac{\partial \eta}{\partial t} + u\frac{\partial \eta}{\partial x}, \tag{6}$$

and since the crest M moves with the phase speed c it follows, combining (5) and (6):

$$\begin{aligned} u_c \left.\frac{d\alpha}{dt}\right|_{M,S} &= -\left(\frac{\partial}{\partial t} + c\frac{\partial}{\partial x}\right)\left(\frac{\partial}{\partial t} + u\frac{\partial}{\partial x}\right)\{\eta\} \\ &= -\mathcal{L}_c \cdot \mathcal{L}_x\{\eta\}, \end{aligned} \tag{7}$$

where $\mathcal{L}$ is the linear convection operator, as indicated.

The wave form for modulating waves has been given by a number of investigators in the deep water case. Yuen and Lake (1982), Li and Tulin (1995), Oshri (1996), and in restricted depth, Mei (1982). Their results, omitting weak current effects, can be put in the general form

$$\begin{aligned} \eta(x,t) = &\quad a(\xi)\cdot\left(1 + \sum_{n=1} \beta_n (ka)^n\right)\cos\Theta \\ &- a_A/\omega \cdot \sum_{n=1} \gamma_n (ka)^{n-\frac{1}{2}} \sin(n\Theta) \\ &+ \quad a(\xi)\cdot\sum_{n=1} \delta_n (ka)^n \cos(n+1)\Theta, \end{aligned} \tag{8}$$

where the sinusoidal wave phase is $\Theta = k(x - ct)$, and the modulation envelope phase is $\xi = k(x - \tilde{c}t)$. The coefficients, $\{\beta_n, \gamma_n, \delta_n\}$, are all functions of ξ and kd, where d is the uniform water depth. The wave celerity is c and the propagation speed of the modulation is $\tilde{c}$. We note, following (8), that

$$A(\xi) = a(\xi)\left[1 + \sum_{n=1} (ka)^n \cdot (\beta_n + \gamma_n)\right]\Big|_K \tag{9}$$

Taking into account that $\Theta = 0$ at M, and that, in general,

$$\mathcal{L}_c\{e^{in\Theta}\} = 0 \tag{10}$$

and that $u_{M,S}$ is a maximum, substituting (8) in (7), we find

$$u_c \dot{\alpha}|_{M,S} = -\left(\frac{\partial^2}{\partial t^2} + uc\frac{\partial^2}{\partial x^2} + (u+c)\frac{\partial^2}{\partial x \partial t}\right)\{A(\xi, kd)\} \tag{11}$$

$$u_c \dot{\alpha}|_{M,S} = \tilde{c}^2(1 - u/\tilde{c})(c/\tilde{c} - 1)A_{\xi\xi}. \tag{12}$$

It is kinematically necessary for $\dot{\alpha}|_{M,S}$ to have the same sign as $A_{\xi\xi}$, so that it is required for the propagation of (8),

$$(1 - u/\tilde{c})(c/\tilde{c} - 1) \geq 0. \tag{13}$$

For naturally occurring wave groups, $\tilde{c} = c_g < c$, and the requirement follows that

$$u/c_g|_{M,S} \leq 1. \tag{14}$$

This analysis, (12), therefore shows that the inviscid propagating wave solution, (8), which is subject to slow modulations, cannot exist for $u_c > c_g$. As the simulations show, the consequence is for the wave shape to quickly deform, and for breaking to follow. The result (12) does suggest an inflection in η_M in the neighborhood of the condition $u_c = \tilde{c}$, and this inflection is observed in LONGTANK simulations, see the wave evolving just after the criterion is reached at the far left in Figure 9, before serious distortion takes place.

3.3 Experimental verification

We have developed an automated, video, particle tracking system for the measurement of surface orbital velocities, Hoyer (1998), and utilized it for a variety of studies, including orbital velocities in mechanically produced wave groups, including breaking waves, and in wind waves, Matsiev *et al.* (2000).

In non-breaking wave groups, the experiments reproduced the kind of orbital trajectories first produced by LONGTANK, and especially the long, flatter, trajectories which appear when passing through the group peak, Figure 18. Notice the unusually long and flat trajectory near breaking. All of these experiments were performed in essentially deep water.

The history of the horizontal velocity in a large number of cases was measured and studied carefully, including some multiple particle tracks, and correlations made with video observations. In this way the OEL breaking criterion could be subjected to verification. The details are to be published separately.

These observations of mechanical wave groups confirm the LONGTANK simulations and the breaking criterion: breaking is initiated only at the modulation peak; for peak orbital velocities, $u_c < c_g$, breaking never occurs; when u_c reaches c_g, breaking is

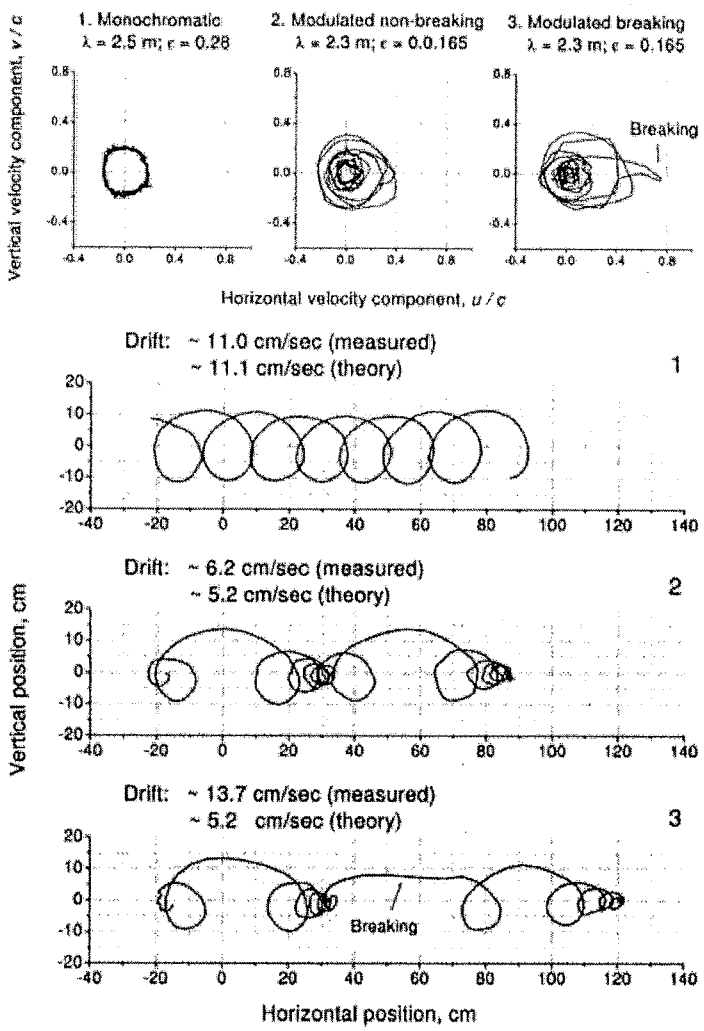

Figure 18: Orbital trajectories in both phase and physical space for different wave conditions.

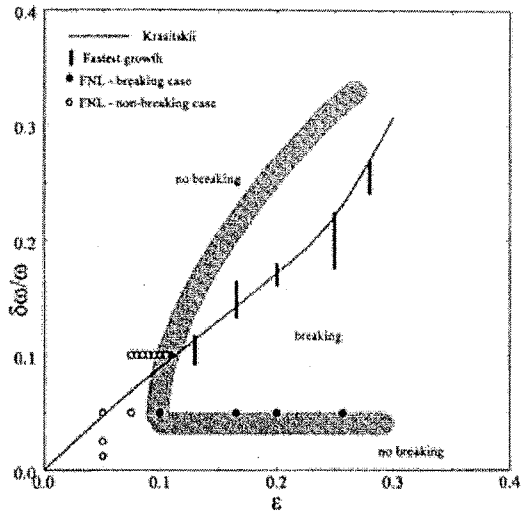

Figure 19: The $(\varepsilon, \delta\omega/\omega)$ diagram, displaying the region where breaking events were observed; $\varepsilon = a_0 k_0$ and $\delta\omega$ is the sideband spacing. Circles are from fully nonlinear computation from Landrini *et al.* (1998). Thick grey line indicates an approximate breaking-nonbreaking boundary as determined from the experiment of Tulin and Waseda (1999).

initiated, and the peak orbital speed quickly increases as deformation proceeds.

3.4 The limits of breaking

The earliest observation of wave breaking in the field, carried out in sheltered water, Weissman *et al.* (1984), revealed mean wave steepness, $a_0 k_0$, much lower than laboratory measurements, and were greeted skeptically. Subsequent North Sea measurements, Holtuijsen and Herbers (1986), revealed even lower breaking steepness, not much larger than 0·1, and Su and Green (1985), found the explanation of breaking at similarly low steepness in wave modulation effects, showing breaking for mean steepnesses as small as about 0·00.

We have found in systematic observations of wave breaking in wave groups, that the characteristics of the modulation also influence breaking, and in particular, the value of the sideband spacing, $\delta\omega/\omega$, used to produce the modulation. In systematic experiments we were able to produce a map of breaking conditions, Tulin and Waseda (1999), see Figure 19. To this experimental map were added data obtained from systematic exact nonlinear simulations, Landrini *et al.* (1998). These studies confirm that breaking in modulated wave groups can occur for mean wave steepness as low as about 0·1, for sideband spacings in the neighborhood of 0·1 - 0·05.

These latter numbers suggest that ocean modulations correspond roughly to the most rapidly growing sidebands, which occur when $\delta\omega/\omega \approx a_0 k_0$ according to instability theory. This lends plausibility to the idea that energetic wind waves in the ocean modulate naturally, and become limited in their steepness soon after breaking first occurs for mean steepness of order one-tenth.

4 THE SIMULATION OF SPLASHING

We briefly describe the Smoothed Particle Hydrodynamics (SPH) method, originally introduced by Lucy (1977) and developed to a high level of maturity by Monhagan and coauthors (Monaghan 1992). More recently, a lot of theoretical studies are becoming available to set on a rigorous basis the convergence of the method (see Di Lisio *et al.* 1998, Moussa and Villa 2000).

The basic idea is to consider a set of N particles with mass m_j distributed over the bulk of fluid Ω, see the example in Figure 20. Each particle is characterized by a kernel δ_ϵ: a kind of shape function which is symmetric, regular, nonnegative, and centered on the particle position, Figure 21. The mass and the other physical information carried by each particle are "smoothed" (averaged) through the kernel over its spatial support.

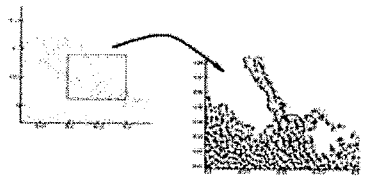

Figure 20: Typical distribution of particles, ∗, in a free-surface flow. In the enlarged detail, the circle represents the radius of interaction of a generic particle.

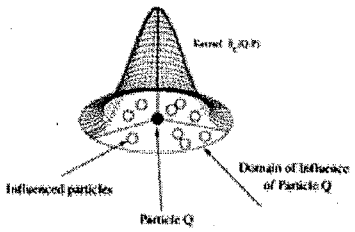

Figure 21: Schematic view of the kernel δ_ϵ centered on the particle Q.

Each particle moves in the force field generated by the whole particle system and the physical quantities evolve according to suitable evolution laws following from the original differential field equations.

The essential feature of the resulting algorithm is the complete absence of a computational grid and, in the present version of the method, a fully Lagrangian character (see Belitschko *et al.* (1994) for a discussion of Eulerian grid-less methods).

4.1 Basic SPH Equations

Let us consider the field $f(P)$ of a physical quantity. A regularized representation of $f(P)$ is given by the interpolation integral

$$\langle f(Q)\rangle = \int_\Omega f(P)\delta_\epsilon(Q-P)\,d\Omega_P \qquad (15)$$

The parameter ϵ represents a measure of the spreading of the kernel over the space and it is assumed that $\delta_\epsilon(Q-P)$ converges to a Dirac delta-function as the parameter $\epsilon \to 0$. It is not necessary, though computationally effective, that the kernel has a compact support (i.e. it is identically zero beyond a certain distance from the particle). In any event, the choice of the kernel is quite important in determining the stability properties of the discrete method (Morris 1997). In our computations we adopted spline kernels either of third or of fifth order, with 30 to 50 particles inside the interaction radius of each particle (*cf.* the circle in Figure 20). The resulting total number of particles depends on the application considered, in some cases being of order of 10^5.

Upon inserting (15) in the Euler Equations, after some manipulations, we get the following evolution equations for the density ρ_i and the velocity $\mathbf{v}_i$ of the i–th particle located at point $\boldsymbol{P}_i$:

$$\frac{d\rho_i}{dt} = +\sum_{j=1}^{N} m_j\,(\mathbf{v}_i-\mathbf{v}_j)\cdot\nabla_i\delta_\epsilon(\boldsymbol{P}_i-\boldsymbol{P}_j)$$

$$\frac{d\mathbf{v}_i}{dt} = -\sum_{j=1}^{N} m_j\left(\frac{p_i}{\rho_i^2}+\frac{p_j}{\rho_j^2}\right)\nabla_i\delta_\epsilon(\boldsymbol{P}_i-\boldsymbol{P}_j)+\boldsymbol{g} \qquad (16)$$

p_i being the pressure. It has to be noted that the fluid has been modeled as a compressible fluid and for real gases an energy equation can be consistently written down. For the present purposes, we will consider a state equa-

tion of the form

$$p = B\left(\frac{\rho^{\gamma}}{\rho_0^{\gamma}} - 1\right) \qquad (17)$$

with $\gamma = 7$ and B tuned to have a negligible compressibility, Monaghan (1992). In practical computations, the largest density fluctuations are of order $10^{-2}\rho_0$. It is worth stressing that the use of a weakly compressible fluid is not unusual in other fields of computational fluid mechanics and, in the present case, it is essential to avoid a wrong evaluation of the smoothed density field when approaching boundaries. Also to be noted is the symmetric structure of the discretized momentum equation which ensures linear and angular momentum conservation.

Finally, an artificial bulk viscosity term has been introduced in the discretized pressure gradient with the sole purpose to increase the stability properties of the numerical algorithm.

The resulting evolution equations can be stepped forward in time by any ODE integrator. In the present case, a second-order predictor-corrector scheme is adopted with a dynamic choice of the time step according to stability constraints. Kinematic constraints, *i.e.* small distance $\boldsymbol{P}_i - \boldsymbol{P}_j$ between particles with respect to $(\boldsymbol{v}_i - \boldsymbol{v}_j)\delta t$, can require easily an extremely small time step δt (not required by the physics or by the stability). Therefore, we employed an individual time-stepping algorithm to let the particles evolve hierarchically according their own time step (Hernquist and Katz 1989).

Some more technical details such as fast searching algorithms for efficient particle interaction, enforcement of boundary conditions by ghost particles and renormalization will not be discussed here, though they play a crucial role in the algorithm. More worth stressing is the great potential of this rather "young" method, which is suitable in principle to handle multi-phase flows, weak compressible effects (acoustics), and surface tension. Also, the extension to three-dimensional flows does not suffer theoretical constraints, though it is computationally demanding.

The numerical method sketched above has been implemented for two-dimensional flows in a code called *SPlasH*. A large variety of applications to violent free-surface flows (notably the dam breaking and sloshing flows with fluid-solid impacts) have been tested, and compared with solutions by other solvers, and will be reported elsewhere.

All the computations presented have been performed by PCs based on Pentium III 700MHz, required 24-72 hours CPU-time and memory never exceeded 50 MBytes.

In the following, we will discuss some model problems to highlight details of the breaking process.

4.2 The Breaking Bore

The model problem is sketched in Figure 22: the flow starts with a semi-infinite layer of fluid, depth h_0, forced into motion by a vertical piston, moving from left to right with constant speed U. At the beginning of the simulation, a smooth ramp-function for the piston velocity has been used to prevent the irrelevant (for our purposes) formation of a jet at the solid boundary.

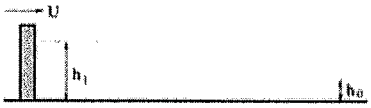

Figure 22: Sketch of the bore generated by a piston moving horizontally with velocity U in a layer of fluid with initial depth h_0. In this case an undular bore is shown.

A typical evolution for $U/\sqrt{gh_0} = 0.8$ is shown in Figure 23, where the particles used in the simulation by *SPlasH* are plotted together with the free surface profiles obtained by a Boundary Element Method (BEM). The particles are colored according to their initial distance from the bottom; this will make easier the description of the breaking events and readily give an idea of the strong mixing process involved. Here, we observe the piling up of the water against the piston and, after a while, a long wave starts to propagate away from the piston with velocity of order $\sqrt{gh_0}$. Actually, for small U, an undular bore would appear (*cf.* Figure 22), smoothly reconciling the initial unperturbed water level with the higher one behind it. In the case here considered, the velocity of the piston is high enough and the wave front breaks soon, leading to one of the most celebrated examples of breaking waves: a breaking bore.

The good agreement between the two solution methods is apparent, though the impact of the falling jet against the underlying free surface prevents the BEM to continue the simulation. Therefore the breaking

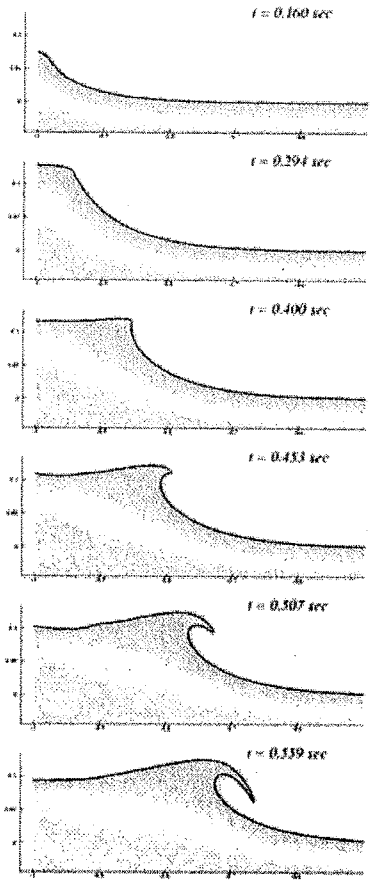

Figure 23: Initial evolution of the free surface motion induced by a vertical piston in steady forward motion, $U/\sqrt{gh_0} = 0.8$. The free surface profiles are obtained by BEM (black solid lines). The particles from *SPlasH* computations are colored according to their initial vertical height.

and post-breaking evolution, given for this case in Figure 24, will be analyzed only by *SPlasH*. In plot A, the plunging jet has just touched the front face of the free surface. The kinematics of the impacting jet will be discussed in better detail later, and here the attention is focused on the splash-up cycles and the genesis of large vortical structures. The closure of the cavity, shown since plot A, originates a first clockwise rotating structure, plots B-C. The impinging jet is also feeding the splash-up *I*, plot B, which grows in the form of a mushroom-like structure, plot C. A second plunging event is already detectable, giving rise to a second clockwise rotating structure, which, with a different rate of growth, assists in the formation of a backward facing jet.

The formation of the mushroom-like structure, and the growth of the backward jet, are essentially related to the gravitational collapse of the mass of water which, deflected upward by the impact, eventually falls down, plots C-D. The further evolution of the backward-facing jet, impacting with the free surface, plot E, results in a counter-clockwise vortex, close to the first one, thus giving origin to a dipole-like structure under the free surface.

In the meantime, the second plunging breaker causes the growth of the splash-up *II*: in plot D a less defined forward plunger is still detectable, while the formation of a second backward facing jet already appears in plot E, eventually leading to a new counter-clockwise vortex, plot G, and forming a second dipole-like structure.

The splash-up *III* in plot F is less vigorous: the forward jet is rather weak and thin and the backward flow, still detectable, is more in the form of a layer of fluid shearing over the clockwise structure originated by *II*. In the following evolution, not shown, we observed other splash-up cycles similar to *III*. Therefore, we have not detected a periodicity for the formation of the dipole-like structures, which requires the appearance of a strong enough backward jet. The strength of the latter, indeed, determines the type of the interaction with the free surface. For more energetic backward jets, a strong rear vortex results, Bonmarin (1989), and a dipole structure is formed, usually propagating below the free surface in our simulations. Air entrapment is likely to occur, with fresh water also captured within the submerging dipole (see the dipole-like structures in plot H). This type of interaction resembles MODE B observed by Bonmarin (*cf.* Bonmarin 1989, Figure 25).

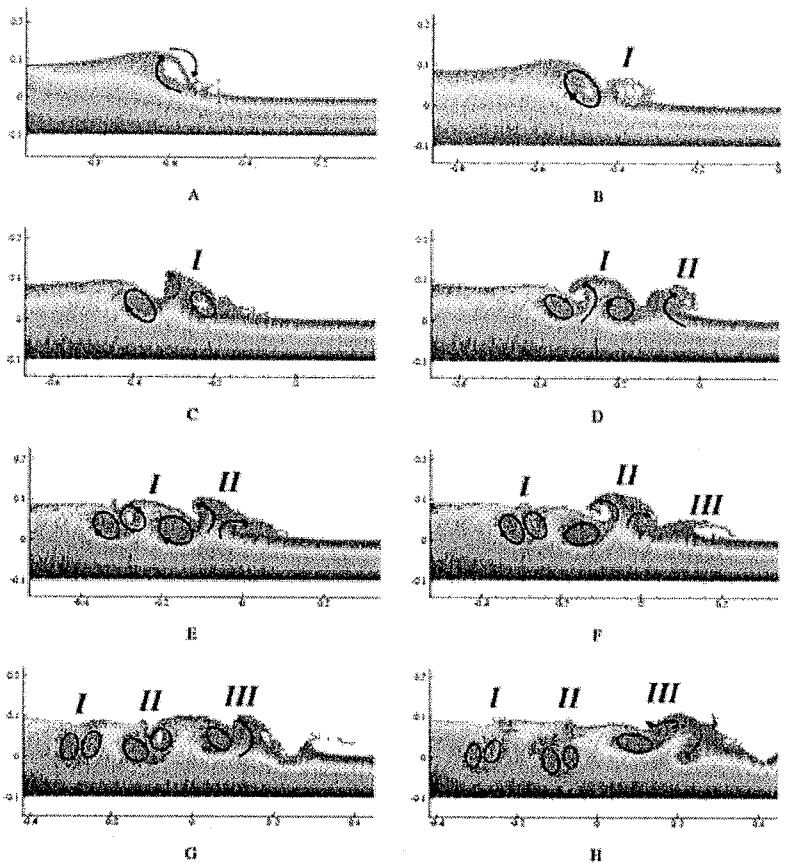

Figure 24: Further evolution of the case presented in Figure 23. Only SPH computations are reported. Plots A through H correspond to t =0·693, 0·853, 1·067, 1·2, 1·28, 1·36, 1·493 and 1·627, respectively. Time is expressed in seconds.

For weaker backward jets, the interaction is more in the form of a layer of fluid surfing on top of the free surface (closer to MODE A in Bonmarin's paper). This is shown in plots G-H where the splash-up *III* divides into forward and backward moving layers, the latter remaining at the surface in a sort of shear layer. In this case, though vorticity of opposite sign is generated, the dipole structure is not well defined and positive and negative vorticity remain closer to the free surface.

In the above description, the genesis of each vortical region is connected with a folding over of the surface to create a doubly connected region and this is crucial to the generation of vorticity and circulation. At the same time air is entrained, which is not accounted for in these calculations, and which can alter the fine details of the evolution. It can be speculated that the downward motion of the dipole structures is altered by buoyancy effects associated with the bubbly phase entrapped into the rotating cavities. SPH can deal with a fluid of varying density and, in principle, it is possible to include such effects, although the accurate estimation of the actual local change in fluid density through local air entrainment is a problem into itself.

Plots in figure 25 give a closer view of the velocity field in the splash-up regions *I* and *III*, respectively. The first shows better the gravitational collapse leading to the formation of an intense backward-facing jet and to MODE B interaction. This back-flow is weaker for splash-up *III*, resulting in a shearing layer on the top of the left-most clockwise structure, MODE A.

The forced breaking bore features repeated plunging events, which is also typical of breaking in shallow water as in the case of wave trains approaching a beach. A detailed description of the first plunging event is instructive, also for deep water breaking waves, and is given through the plots of Figure 26.

In particular, we have chosen the reference configuration in the top-left plot and we have assumed that the jet is formed by those particles within the area delimited by the free surface and the vertical line tangent to the nascent loop beneath the jet. These particles are colored in black. In the following plots the motion of these particles is easily tracked, thanks to the Lagrangian character of the SPH. During the free falling phase, because of mass conservation, the jet is stretched and reduced in thickness. At impact, the jet-particles flow into two separated streams, plot C. One is deflected

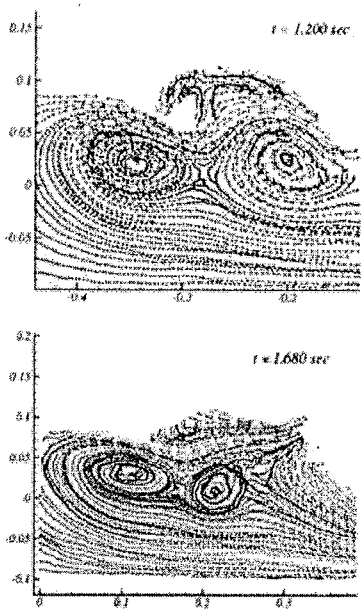

Figure 25: Close view of the velocity field in the splash-up. Top: MODE B interaction for splash-up *I* in Figure 24. Bottom: MODE A interaction for splash-up *III* in Figure 24. Black arrowed lines give an indication of the overall direction of motion.

inside the loop, and the other one contributes to the formation of the splash-up. Up to this point, the plunger is still fed only by fresh particles (colored in red, plot D) which will undergo the same evolution as the black particles. In later stages, the particles earlier entrapped by the clockwise structure, will complete one revolution and (partly) re-contribute to the impinging jet, plots D-E, implying a strong mechanical mixing.

Those particles, earlier entering the splash-up, now evolve into a new plunger and are again split into a portion captured by a second clockwise structure and a remaining one forming the splash-up *I* in plot C of the previous Figure 24.

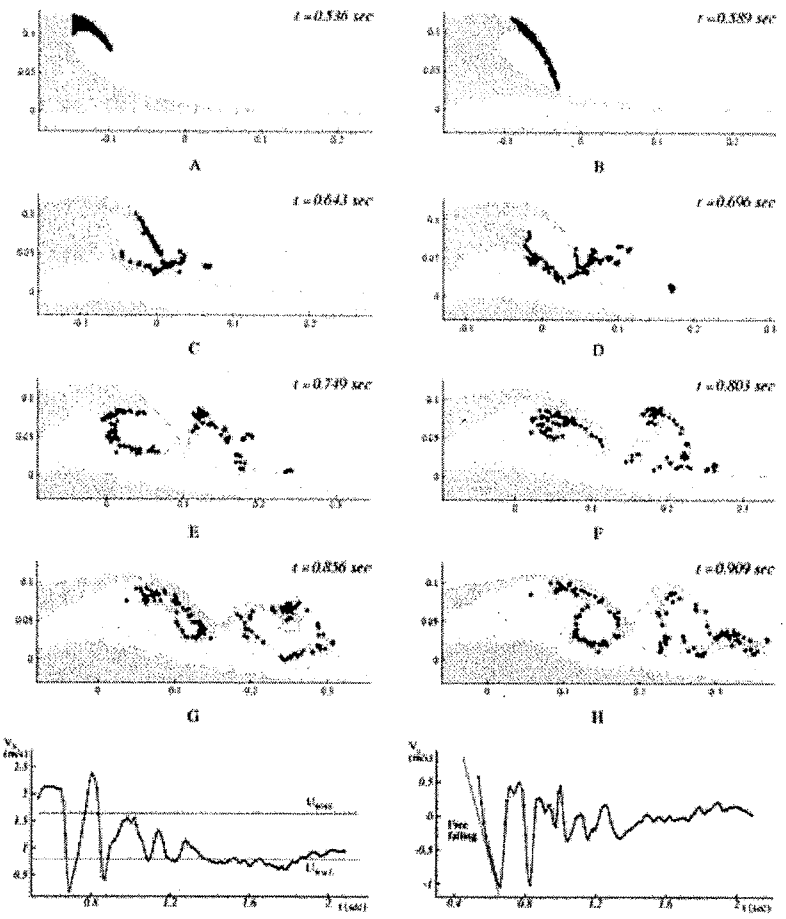

Figure 26: Evolution of the particles originally forming the jet (marked by black symbols). The two bottom diagrams show the time evolution of the horizontal (left) and of the vertical (right) components of the fluid momentum within the jet.

It can be seen, that a portion of the particles originally in the first plunger are now riding on the moving front of the propagating wave, while the others are captured by the cavities and effectively mixed with other portions of fluid. In following cycles, all the tracked particles will be captured by the rotating structures and fresher particles will feed the bore front.

A more quantitative analysis is obtained by the two bottom plots, where the components of the velocity of the center of mass of the jet-particles

$$\boldsymbol{V}_c = \int_{jet} \rho \boldsymbol{v}\, dA \Big/ \int_{jet} \rho\, dA \qquad (18)$$

are plotted in time. The free fall stage in the first part of the jet-evolution can be clearly seen in the right plot, and accompanied by an almost steady translation in the horizontal direction (*cf.* left plot). The instant of the impact is evidenced by the sharp changes of $V_{c,x}, V_{c,y}$. The first drops down to less than 25% of its initial value: this corresponds to the splitting of the jet into two portions with backward and forward motion, balancing each other and thus reducing $V_{c,x}$. The vertical component bounces up, changing in sign, because both portions are moving upward, and then oscillates consistently with the orbital motion of the particles entrapped in the cavities. Eventually, $V_{c,y}$ attains an almost zero value, with small amplitude oscillations related to the orbital motion inside the vertical structures rotating in an uncorrelated way. After some oscillations with decreasing amplitude, due both to the orbital motion and to the multiple splash-up, the horizontal component attains the uniform velocity of the moving piston.

We have analyzed several cases, in the range $U/\sqrt{gl_0} \in [0.5, 0.95]$. For larger U, a more vigorous formation of the backward plunging jet and MODE B interaction has been observed, with initial formation of stronger dipole-like structures, followed by a predominance of MODE A interaction with vertical regions more confined to the free surface. A slower motion of the piston leads to less pronounced splash-up cycles, producing weaker vertical structures of opposite sign, mainly due to MODE A interaction. In the present simulations, for $U/\sqrt{gl_0} \leq 0.6$, dipole-like structures are never observed. In all cases, MODE B appears connected with the initial breaking events, when the most energetic plungers are generated.

Plots in Figure 27 give an indication of this transformation by comparing some global characteristics of the plunging jet and those of the corresponding splash-up, for two values of the piston velocity $U = \sqrt{gl_0}$. Many parameters are involved and we simply report some of them, just to show the complexity of the underlying dynamics involved. All the quantities are referred to a unit slice of fluid in the direction orthogonal to the plane of motion. The mass in the jet at the touch down is 2.55 kg and 0.618 kg for the two cases, respectively, and the corresponding cavity entrapped is 45.4 cm^2 and 13.9 cm^2. Despite the rather large differences in jet masses, the masses involved in the splash-ups are comparable: 4.51 kg and 3.45 kg. This is probably due to the difference in the impacting angle (21.1° *vs.* 18.6°), implying different depths of penetration of the jet. It is remarkable that the mass of

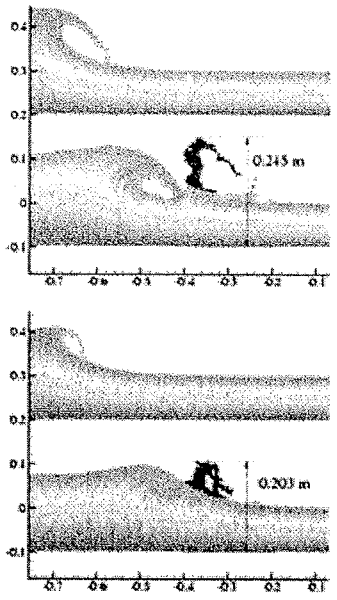

Figure 27: The first plunging event and the corresponding splash-up for $U/\sqrt{gl_0} = 0.95$ (top) and $U/\sqrt{gl_0} = 0.7$ (bottom). The configuration of the splash-up is reported when the upward-raised water reaches the maximum height.

the splash-up is greater than the original jet which gave rise to it.

The entire history of the bore from initiation of the motion involves the pile up of the water at the piston, the propagation of the wave, overturning and initial splashing followed by a series of splashes. Finally the splashes ceases and a surfing eddy remains on the face of the equilibrium bore, analogous to the breaker above a hydrofoil, Figure 1; this was observed in our simulations and in experiments reported by Peregrine (1983). In this condition, the velocity of the breaking front attains a constant value; *i.e.*, in the frame of reference of the front, the velocities far upstream and sufficiently downstream are constant.

For hydraulic jumps, by using mass and momentum conservation principles, we can relate the dimensionless velocity of the bore

$$F_0^2 = (\frac{v_{th}}{\sqrt{gh_0}})^2 = \frac{1}{2}\left(\frac{h_1}{h_0}\right)\left(1+\frac{h_1}{h_0}\right) \qquad (19)$$

to the upstream, h_0, and downstream, h_1, water levels. In Table 1, data from *SPlasH* simulations are collected and compared with the theoretical prediction. The agreement is generally within 1%, and 2% at maximum, quite reasonable for such complex, non-steady dissipating flows.

$U/\sqrt{gh_0}$	h_1	h_1/h_0	F_0	v_{th}	v_{xprim}
0·95	0·212	2·12	1·62	1·69	1·61
0·9	0·21	2·1	1·8	1·78	1·78
0·8	0·19	1·9	1·66	1·64	1·63
0·7	0·18	1·8	1·59	1·57	1·57
0·6	0·17	1·7	1·52	1·50	1·47
0·5	0·15	1·5	1·37	1·36	1·38

Table 1: Comparison between the computed velocity, v_{xprim}, of the bore front and the theoretical value, v_{th}, predicted by global mass and momentum conservation principles, *cf.* Equation (19). Velocities are expressed in m/s.

The result strongly suggests that inertial (Euler) effects may dominate the observable phenomena, including strong mixing of surface water when passing through the bore.

4.3 Breaking Bow Waves

Breaking ship waves have always captured the interest of hydrodynamicists and naval architects because of their role in contributing to the resistance of the hull. More recent, however, is the interest of the Navy in the very long narrow wakes behind ships which can be observed remotely, and which originate abeam the ship through extensive breaking of diverging bow and stern waves.

The following analysis of this problem is limited to fine ships with a sharp stem, for which fundamental understanding can be gained by an approximate quasi-three dimensional model based on the idea that longitudinal gradients of relevant flow quantities are small compared with vertical and transverse gradients. The introduction of this seminal idea is not new, and a historical recollection of slender-body theory for ship hydrodynamics is given by Maruo (1989) and by Fontaine and Tulin (1998).

More specifically relevant to our purposes, nonlinear versions of this parabolized model for ship flows have been presented by Faltinsen and Zhao (1991), Maruo and Song (1994) and Tulin and Wu (1996). In the last two, the calculations are carried out in two dimensions, vertical and transverse, and successively in time and the method has been consistently named 2D+t.

Tulin and Wu (1994) presented a thorough analysis of the genesis of diverging bow waves, and a detailed parameter investigation is reported in Wu (1997). In particular, the method exhibited the advantage of high resolution, sufficient to capture breaking, and even to trace the jet overturning.

An example of this ability is presented in Figure 28, where free surface profiles for successive time-steps are superimposed, showing one of the key features of the slender-hull bow wave system: the *splash*. Tulin and Wu (1994). For this ship (a Wigley hull), the free-surface flow is not much decelerated before the stem, but upon reaching it, is deviated sharply upwards, rises on and eventually levels off and falls down. An entire thin sheet is formed in this process and appears as a splash on either side of the hull. The relaxation of these splashes is the prime source of divergent waves. In the present case, the large beam-to-length ratio, $B/L = 0{\cdot}2$, makes the radiated waves large enough to break, following an evolution similar in many ways to that described in Sections 2-3, with crest-rising, front-steepening and jet formation.

Some genuine three-dimensional effects, such as upstream influence and breaking before the bow, become increasingly important as the ship becomes full

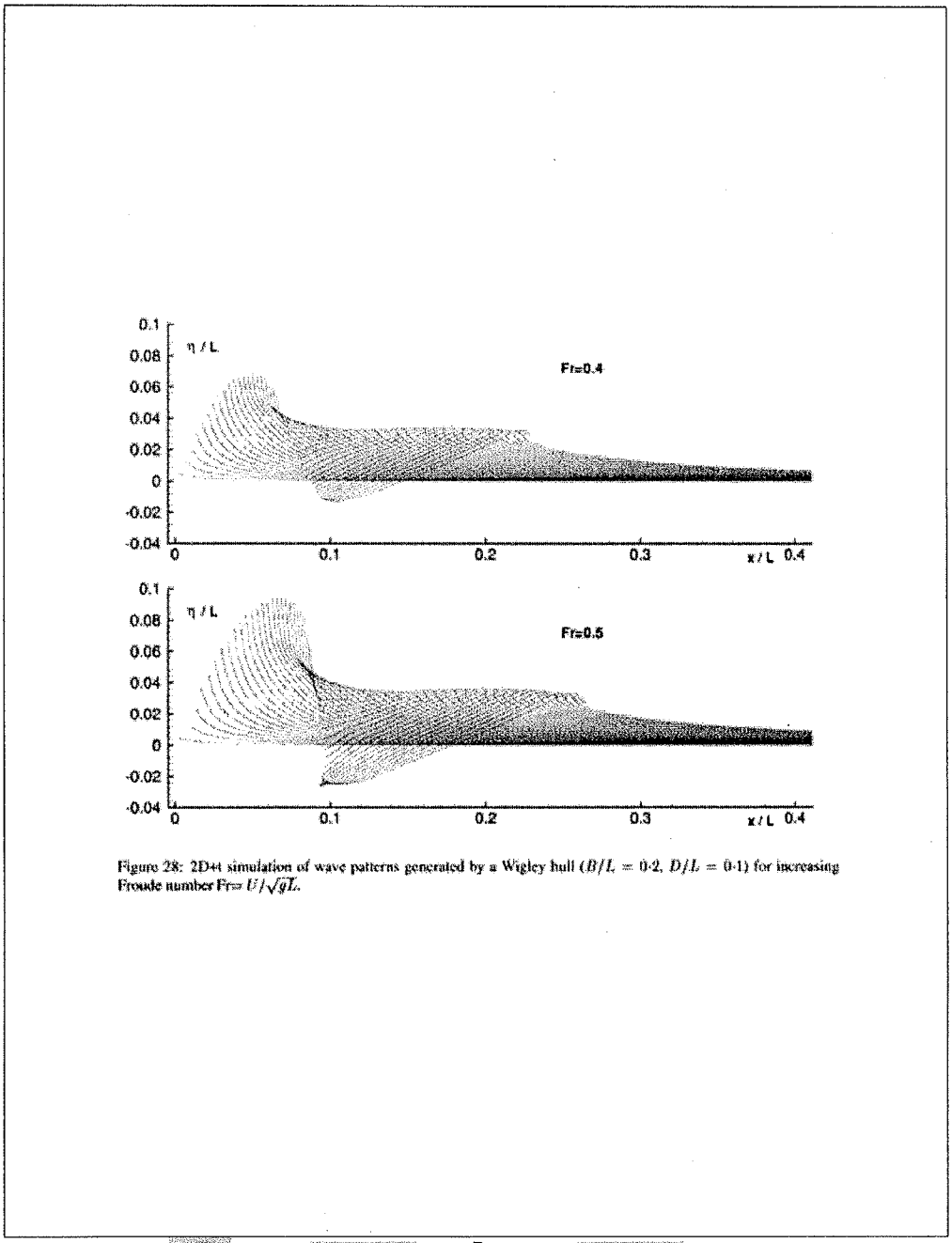

Figure 28: 2D+t simulation of wave patterns generated by a Wigley hull ($B/L = 0{\cdot}2$, $D/L = 0{\cdot}1$) for increasing Froude number $Fr = U/\sqrt{gL}$.

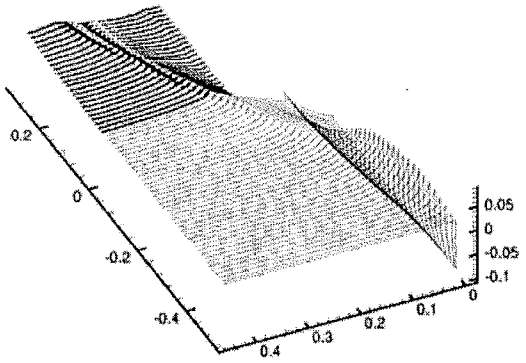

Figure 29: Perspective view (from upstream) of the wave pattern generated by a Wigley hull ($B/L = 0{\cdot}1$, $D/L = 0{\cdot}1$, $Fr = 0{\cdot}46$). BEM computation (blue lines) starts from the bow, up to $x/L = 0$. Black solid lines are made by the uppermost layer of fluid particles from *SPlasH* computations, initialized by BEM.

and slow and are lost to this parabolized theory.

In the following we apply a version of *SPlasH* to study the splashing of the forward wave generated by a Wigley hull. The computation is initiated by a 2D+t code based on BEM, and continues up to the detection of jet overturning. Once this is accomplished, a subdomain, surrounding the breaking area, is defined and filled in with particles. The initial velocity and pressure of the particles is determined by BEM but, so far, we have not fully coupled the two algorithms and, on the outer SPH boundary, stationary conditions have been imposed during all the following evolution. Therefore, preliminary sensitivity tests have been conducted to determine the vertical and horizontal dimensions of the SPH domain to assure the invariance of the results during the entire simulation time.

A perspective view of this compound simulation is presented in Figure 29. The view point is located upstream the bow, and $y - z$ configurations for increasing time are plotted in a 3D fashion by using $x/L = Ut/L$ as longitudinal coordinate, with the origin located midship. Ship cross sections (red lines) are plotted only for those slices obtained by BEM, and the corresponding free surfaces are represented by blue lines. For this Froude number, Fr=0·46, we observe a substantial splash at the bow, with height comparable with the draft and maximum located around 25% L from the stem line. The gravitational collapse of the splash is accompanied by the radiation of a wave, which steepens and forms a plunging jet, almost touching the free surface for $x/L = 0$.

From this configuration on, the SPH computation has been started and the resulting free-surface pattern is reported in the same figure by black lines. Only the layer of particles at the free surface is plotted and its horizontal extent corresponds to the actual computational domain used by *SPlasH*.

A more detailed analysis is given in Figure 30, where an enlarged view of the wave pattern during the splash (top) is presented together with some selected particle distributions (bottom). Upon adopting a stern viewpoint, we observe that the breaking crest is propagating with an almost unchanged phase speed, though the simulation time is rather short to be conclusive and

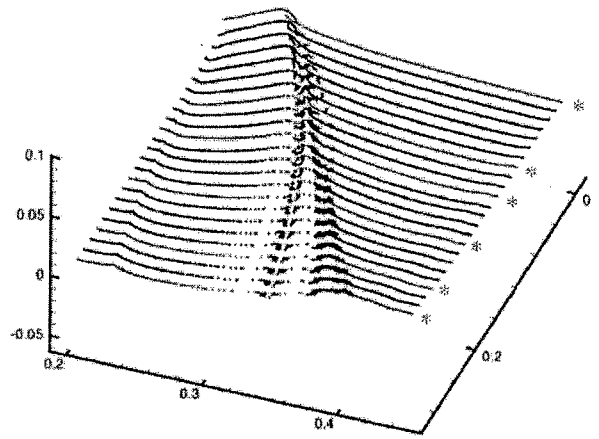

Figure 30: Breaking of the bow wave generated by a Wigley hull ($B/L = 0.1$, $D/L = 0.1$, $Fr = 0.16$). Details from Figure 29. Only the uppermost layer of particles from *SPlasH* computations is plotted. Red colored sections are reported in Figure 31.

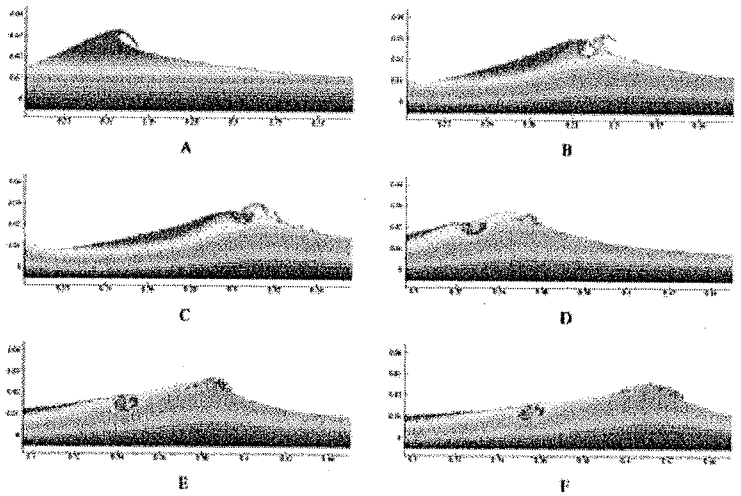

Figure 31: Particle distributions from Figure 30 showing splashing and formation of vortical regions.

the analysis hampered by the spreading of particles around the crest emerging from the breaker.

More clear is the presence of a slower trace, originating from the splash-up, and left on the free surface behind the breaking crest. The analysis of particle distributions, colored according to the vertical distance from the highest point, reveals its origin. The impacting jet, plot A, causes splash-up and cavity formation, plot B. A backward-facing jet is created, with a MODE B interaction, plot C, and eventually resulting in a dipole structure left behind the propagating crest, plot D through E. This dipole is weaker with respect to those observed for breaking bores with large U. Furthermore, the overall downward-backward motion of the fluid past the crest corresponds to the possible self-convection of the dipole, which remains close to the free surface. In any case, because of its vortical nature, the dipole structure does not follow the breaking crest, leaving its own signature on the free surface.

An analysis of the motion of the particles initially forming the plunging jet shows strong similarities with that presented in Figure 26, for the breaking bore. Also in this case, the jet flows in a backward stream, captured in the nascent cavity, and another one feeding the splash-up. It is worth stressing, in this case, that the fluid particles emerging forward from the splash-up in plots B-C, are then "surfing" the wave crest after the splashing event, plots D-F, thus resembling the weak eddy steadily moving with the hydrofoil breaking wave, as discussed at the beginning of this paper.

We found a striking similarity between the present results and the experimental observations by Lamarre, reported in Melville (1996, Figure 2). Clearly, on a longer time scale, the degassing stage will be profoundly effected by the two-phase nature of the bubbly flow created during the breaking.

For bow-flared ships and practical Froude numbers, wave breaking takes place much closer to, or at the bow. This has been shown in Tulin and Wu (1996, Figure 13), where the first stage of the gravitational collapse of the splash at the bow, with formation of a strong plunger, has been computed for a frigate ship.

Although the application of the SPH technique to study these flow conditions requires some improvements (e.g. modeling of curved boundaries, and matching with an outer solution for long-time simulations), we can already get some basic insights by considering the flow forced by an inclined piston. In particular, we

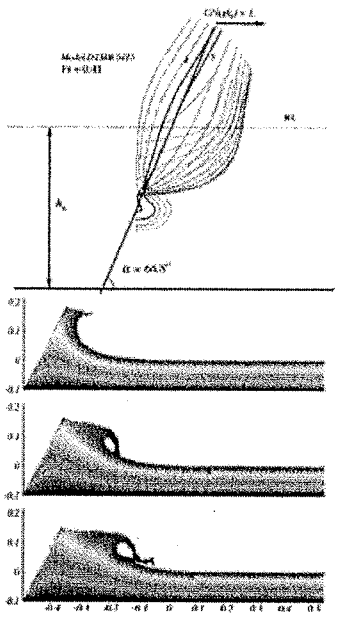

Figure 32: Top: sketch of the model problem adopted to study a breaking splash. Bottom plots: evolution of the splash breaking near the piston. Jet particles are marked in black to put in evidence the ricochet.

selected an angle of 66.8° by taking the slope at the waterline of the DTMB Model 5415 (*cf.* top plot in Figure 32) in the bow region. In our simulations we used a constant horizontal velocity, $U/\sqrt{gh_0} = 1.0$. For the actual ship and Fr=0.41, the expansion velocity of bow cross sections is even higher but drops down sharply. In the bottom plots of Figure 32, we observe a quick piling up of the water against the piston, with a maximum run-up of about $2h_0$, and the formation of a rather thick jet, eventually collapsing down in the form of a plunger. In contrast to previous results, the impacting fluid is not creating a crater, even though a portion of the impacting jet is still deflected inside the nascent cavity. The evolution on a longer time scale is significantly effected by finite depth, and is less relevant to the ship problem.

Much remains to be done on ship breakers but the present results are very encouraging.

ACKNOWLEDGEMENTS

The ONR sponsors have been gratefully acknowledged in the Forward. I would mention especially our constructive relationship with Dr. Ed Rood, who provided the incentive for the present splashing studies.

Among the many OEL researchers who have contributed to our understanding of breaking waves I would specifically mention four of those who not only received their PhD's at UCSB, but stayed on as Post Graduate Researchers: Pei Wang (Mrs. Y.T. Yao), who conceived of the special domain decomposition technique and implemented it for the high resolution simulation of long wave trains and the breaking process- she is the Mother of LONGTANK: Yi Tao Yao, who utilized LONGTANK so brilliantly in studies of wave breaking, who discovered the breaking criterion, simulated surface tension effects, and who collaborated in a host of studies of ocean wave behavior; J.J. Li, who made many deep and scholarly mathematical studies of wave dynamical behavior in connection with ocean wave modeling; Takuji Waseda, who developed much of our experimental systems for wind wave studies, pioneered in the development of our experimental wave group capability, and carried out a series of profound experimental studies of wave breaking; Ming Wu, who continued the $2D + t$ simulations of ship bow waves initiated by Maruo and Song, and used them intensively and fruitfully in systematic studies of bow waves and of deck wetness.

I am very grateful to my old colleague, Professor Hajimi Maruo, of Yokahama, for spending two productive years at the OEL, during which time the $2D + t$ simulations were begun. I must also thank Dr. Emmanuel Fontaine, now of IFP in Paris, for his vital role while a visiting researcher at the OEL in initiating our work on gridless Euler simulations, and his early explorations and use of the SPH method in splashing studies.

I thank my colleague and co-author Maurizio Landrini for agreeing to the present collaboration which brings him from Rome to the OEL for six months a year, together with Andrea Colagrossi of Rome, who has participated in many of the *SPlash* computations. The successful collaboration was made possible only through the agreement of Admiral U. Grazioli, the President of INSEAN, and of Dr. U. Bulgarelli, the Scientific Director, to whom we are grateful. Finally, many thanks to the tireless staff of the OEL, who have helped in the preparation of this paper, and especially Ms. Sandra Jeppesen, and Mr. Daniel Matsiev.

REFERENCES

Belytschko T., Lu Y.Y. and Gu L. (1994), Element free galerkin, *Int. J. Num. Meth. Eng.*, Vol. 37, pp. 229-256.

Benjamin B.T and Feir J.E. (1967), The disintegration of wave trains in deep water, *J. Fluid Mech.*, Vol. 27, pp. 417-430.

Benney D.J. and Newell A.C. (1967), The propagation of nonlinear wave envelopes, *J. Math. Phys.*, Vol. 46, pp. 133-139.

Bonmarin P. (1989), Geometric properties of deep-water breaking waves, *J. Fluid Mech.*, Vol. 209, pp. 405-433.

Colote R. and Tulin M.P. (1994), A theory of steady breakers, *J. Fluid Mech.*, Vol. 276.

Di Lisio R., Grenier E. and Pulvirenti M. (1998), The convergence of the SPH Method, *Computers Math. Applic.*, Vol. 35, No. 1/2, pp. 95-102.

Dold J.W. and Peregrine D. H. (1986), Water-wave modulation, *Proc. 20th Int. Conf. on Costal Eng.*, Taipei, Vol. 1, pp. 163-175.

Dommermuth D., and Mui R. (1996), The vortical structure of a near breaking gravity-capillary wave, *Proc. 20th ONR Symp. on Naval Hydrodynamics*, pp. 551-567, Natl. Academy Press.

Donelan M., Longuet-Higgins M.S and Turner J.S. (1972), Periodicity in Whitecaps, *Nature*, Vol. 20, pp. 449-451.

Duncan J. (1983), The breaking and non-breaking wave resistance of a two dimensional hydrofoil, *J. Fluid Mech.*, Vol. 126, pp. 507-520.

Duncan J., Philomin V., Qiao H. and Kimmel J. (1994), The formation of a spilling breaker *Phys. of Fluids*, Vol. 6.

Duncan J., Philomin V., Qiao H. (1996), The transition to turbulence in a spilling breaker, *Proc. 20th ONR Symp. on Naval Hydrodynamics*, pp. 530-567, Natl.

Academy Press.

Ebuchi N., Kawamura H., and Toba Y. (1987), Fine structure of laboratory wind-wave surfaces studied using an optical method, *Boundary-Layer Meteorology*, Vol. 39, pp. 133-151.

Faltinsen O.M. and Zhao R. (1991), Flow predictions around high-speed ships in waves, *Mathematical Approaches in Hydrodynamics* (ed. T. Miloh), SIAM, pp. 265-288.

Fontaine E. and Tulin M.P. (1998), On the prediction of free-surface flows past slender hulls using the 2D+t theory: the evolution of an idea, In NATO RTO-MP-15, *Proc. of Fluid Dynamic Problems of Vehicles Operating Near or in the Air-Sea Interface*, Amsterdam.

Fuchs, J. and Tulin, M.P. (2000), Experimental scatterer characterization: the importance and nature of compact scatters in LGA imaging of the ocean, emphasizing microbreakers. Presented at a NATO Symposium on low grazing angle clutter, APL, April 2000. Also OEL Tech. Rpt. No. 00-218.

Goda Y. (1976), On wave groups, *Proc. 1st Intl. Conf. Behavior of Offshore Structures*, BOSS, pp. 115-128.

Hara T. and Mei C.C. (1991), Frequency downshift in narrowbanded surface waves under the influence of wind, *J. Fluid Mech.*, Vol. 230, pp. 429-477.

Hasselman K. (1962), On the non-linear energy transfer in a gravity-wave spectrum, Part 1, General theory, *J. Fluid Mech.*, Vol. 12, pp. 481-500.

Hernquist L. and Katz N. (1989), TREESPH: a unification of SPH with the hierarchical tree method, *The Astrophysical J. Supp. Ser.*, Vol. 70, pp. 419-446.

Holthuijsen L.H. and Herbers T.H.C. (1986), Statistics of breaking waves observed as whitecaps in the open sea, *J. Phys. Ocean.*, Vol. 16, pp. 290-297.

Hoyer K. (1998), Documentation for the particle tracking velocimetry, OEL Tech. Rpt. No. 98-177.

Inui T., Kajitani H. and Miyata H. (1979), Experimental investigation of the wave making in the near field of ships *J. Soc. Naval Arch. Japan*, Vol. 173.

Ivanov A. and Gershenzon, V. (1993), Sea surface wave investigations with a stationary doppler radar, unpublished.

Kjeldsen S.P. and Myrhaug D. (1980), Wave-wave interactions, current-wave interactions and resulting extreme waves and breaking waves, *Proc. 17th Coastal Eng. Conf.*, pp. 2277-2303.

Kjeldsen S.P. (1990), Breaking waves, In: *Water Wave Kinematics*, (Eds.: Torum A. and Gudmestad O.T.), Kluwer Academic Publishers, pp. 453-473.

Komen G.J., Cavaleri L., Donelan M., Hasselmann K., Hasselmann S. and Janssen P.A.E.M. (1994), *Dynamics and Modelling of Ocean Waves*, Cambridge University Press.

Lake B.M. and Yuen H.C. (1977), A note on some nonlinear water wave experiments and the comparison of data with theory, *J. Fluid Mech.*, Vol. 83, pp. 75-81.

Lake B.M, Yuen H.C, Rungaldier H. and Ferguson W.E. (1977), Nonlinear deep-water waves: theory and experiment. Part 2, Evolution of a continuous wave train, *J. Fluid Mech.*, Vol. 83, pp. 49-74.

Landrini, M., Oshri, O., Waseda, T., and Tulin, M.P. (1998), Long time evolution of gravity wave systems. *Proc. 13th Intl. WorkShop on Water Waves and Floating Bodies (Delft)*, (A.J. Hermans, ed.), pp. 75-78. Also OEL Tech. Rpt. No. 98-175.

Li J.J. and Tulin M.P. (1992), On the breaking of energetic waves *Int. J. Offshore and Polar Eng.*, Vol. 2, No. 1.

Li J.J. and Tulin M.P. (1993), Wind forcing and breaking dissipation effects on nonlinear evolution of energetic wave groups, *The Air-Sea Interface*, (Eds. Donelan *et al.*). Distributed by The Univ. of Miami, ISBNO-930050-00-2.

Li J.J. and Tulin M.P. (1995), Nonlinear mechanics of gravity waves on deep water-on the nonlinear Schrodinger equation, *Potential Flow of Fluids*, Chapter 3, *Intl. Series on Adv. in Fluid Mech.*, Computational Mechanics Publication, Boston. ISBN 1.56252.279.5

Longuet-Higgins M.S. (1969), On wave breaking and the equilibrium spectrum of wind generated waves, *Proc. Roy. Soc. London*, Vol. 310A, pp. 151-1.

Longuet-Higgins M.S. and Fox M.J.H (1977), Theory of the almost-highest wave: the inner solution *J. Fluid Mech.*, Vol. 80, pp. 721-741.

Longuet-Higgins M.S. (1985), Acceleration in steep gravity waves *J. Phys. Ocean.*, Vol. 15, pp. 1570-1573.

Longuet-Higgins M.S. (1996), Progress toward un-

derstanding how waves break, *Proc. 21st ONR Symp. on Naval Hydrodynamics*, (Trondheim), National Academy Press, Washington D.C.

Lucy L.B. (1977), A Numerical Approach to the Testing of Fission Hypothesis, *Astronomical Journal*, Vol. 82, No.12, pp. 1013-1024.

Maruo H. (1989), Evolution of the theory of slender Ships, *Ship Tech. Res.*, Vol. 36, pp. 107-133.

Maruo H. and Song W. (1994), Nonlinear analysis of bow wave breaking and deck wetness of a high speed ship by the parabolic approximation, *Proc. 20th ONR Symp. on Naval Hydrodynamics*, Santa Barbara, National Academy Press, Washington D.C..

Matsiev D., Hoyer K. and Tulin M.P. (2000), Surface Lagrangian velocity measurements for breaking and non-breaking modulated waves, OEL Tech. Rpt. No. 00-221.

Mei C.C. (1982), *The Applied Dynamics of Ocean Surface Waves*, Chapter 12, World Scientific: Singapore.

Melville W.K. (1982), The instability and breaking of deep-water waves, *J. Fluid Mech.*, Vol. 115, pp. 165-185.

Melville W.K. (1996), The role of surface-wave breaking in air-sea interaction, *Ann. Rev. Fluid Mech.*, Vol. 28, 1996, pp. 279-321.

Miyata H. (1980), Characteristics of nonlinear waves in the near field of ships and the effects on resistance, *Proc. 13th ONR Symposium on Naval Hydrodynamics (Tokyo)*, Natl. Academy Press.

Monaghan J.J. (1992), Smoothed Particle Hydrodynamics, *Ann. Rev. Astron. Astroph.*, Vol. 30, pp.543-574.

Morris J.P. (1997), Stability properties of SPH, *Publ. Astron. Soc. Aust.*, Vol. 13.

Moussa B.B. and Villa J.P. (2000), Convergence of SPH Method for Scalar Nonlinear Conservation Laws, to appear in *SIAM J. Numerical Analysis*.

Ochi M.K. and Tsai C.M. (1983), Prediction of occurrence of breaking waves in deep water, *J. Phys. Ocean.*, Vol. 13, pp. 2009-2019.

Oshri O. (1996), Frequency downshifting in surface waves, *PhD Dissertation, UCSB*, OEL Tech. Rpt. No. 96-144.

Peregrine D.H. (1981), The fascination of fluid mechanics, *J. Fluid Mech.*, Vol. 106, pp. 59-80.

Peregrine D.H. (1983), Breaking waves on beaches, *Ann. Rev. Fluid Mech.*, Vol. 15, pp. 149-178.

Phillips O.M. (1960), On the dynamics of unsteady gravity waves of finite amplitude, Part 1. The elementary interactions, *J. Fluid Mech.*, Vol. 9, pp. 193-217.

Ramberg S.E. and Griffin O.M. (1987), Laboratory studies of steep and breaking deep-water waves, *J. Waterway, Port, Coastal, Ocean Eng.*, Vol. 113, pp. 493-506.

Rye H. (1974), Wave group formation among storm waves, *Proc. 14th Intl. Conf. Coastal Eng.*, Vol. 1, pp. 164-183.

Smith M.N., Poulter E.M. and McGregor J.A. (1993), Breaking wave groups in developing seas: doppler radar measurements of intermittency, *Proc. 2nd Air-Sea Interface* Conf. (Marseille).

Smith M.N., Poulter E.M. and McGregor J.A. (1996), Doppler radar measurements of wave groups and breaking waves, *J. Geoph. Res.*, Vol. 101, pp. 14269-14282.

Stansberg C.T. (1991) Extreme wave asymmetry in full scale and model scale experimental wave trains, *Proc. OMAE*, Vol. 1-A, pp. 215-222.

Su M.Y, Bergin M., and Bales S. (1982), Characteristics of wave groups in storm seas, *Proc. Ocean Structural Dynamics Symposium*, pp. 118-132, Corvallis, Oregon.

Su M.Y, Bergin M., Marler P. and Myrick R. (1982), Experiments on nonlinear instabilities and evolution of steep gravity-wave trains, *J. Fluid Mech.*, Vol. 124, pp. 45-72.

Su M.Y. and Green A.W. (1985), Wave breaking and nonlinear instability coupling, In: *The Ocean Surface*, (Eds. Y. Toba and H. Mitsuyasu), D. Reidel Publishing Company, pp. 31-38.

Su M.Y. (1986) Large, steep waves, wave grouping and breaking, *Proc. 16th ONR Symp. Naval Hydrodynamics*, pp. 78-92, National Academy Press.

Swamp Group (1985), *Ocean Wave Modeling*, Plenum Press, New York. ISBN 0-306-41685-9.

Trulsen K. and Dysthe K. (1990), Frequency downshift through self modulation and breaking, *Water Wave*

Kinematics, (Eds.: Torum A. and Gudmestad O.T.), Kluwer Academic Publishers, pp. 56-572.

Tulin M.P., Yao Y.T. and Wang P. (1994), The simulation of the deformation and breaking of ocean waves in wave groups, *Proc. 7th Intl. Conf. Behavior Offshore Struct.*, BOSS '74, Elsevier, Amsterdam, pp. 383-392.

Tulin M.P. (1996), Breaking of ocean waves and downshifting, In: *Waves and Nonlinear Processes in Hydrodynamics*, (Eds.: J. Grue and B. Gjevik and J. E. Weber), Kluwer Academic Publishers, pp. 177-190.

Tulin M.P. and Wu M. (1996), Divergent bow waves, *Proc. 21st ONR Symp. on Naval Hydrodynamics*, (Trondheim), National Academy Press, Washington D.C., pp. 99-117.

Tulin M.P. (1997), Remarks on energy transport in waves *Proc. 12th Intl. Work. Water Waves and Floating Bodies*, also OEL Tech. Rpt. No. 97-152.

Tulin M.P. and Li J.J. (1999), The nonlinear evolution of wind driven, breaking ocean waves: mathematical description, OEL Tech. Rpt. No. 99-202.

Tulin M.P. and Waseda T. (1999), Laboratory observations of wave group evolution, including breaking effects, *J. Fluid Mech.*, Vol. 378, pp. 197-232.

Wang P., Yao Y. and Tulin M.P. (1994), Wave-group evolution, wave deformation and breaking: simulation using LONGTANK, a numerical wave tank, *Int. J. Offshore and Polar Eng.*, Vol. 4, pp. 200-205.

Wang P., Yao Y. and Tulin M.P. (1995), An efficient numerical tank for nonlinear water waves, based on the multi-subdomain approach with BEM, *Int. J. Num. Meth. Fluids*, Vol. 20, pp. 1315-1336.

Weissman M.A., Atakturk S.S., and Katsonis, K.B. (1984), Detection of breaking events in a wind generated wave field, *J. Phys. Ocean.*, Vol. 14, pp. 1609-1617.

Welch S., Yao Y., Tulin M.P. and Jaganathan S. (1996), An experimental and numerical investigation of wave loads on floating bridges, including non-linear and wind effects, *Proc. 6th Int. Offshore and Polar Eng. Conf.*, Vol. 3, pp. 228-236.

Welch S., Levi C., Fontaine E. and Tulin M.P. (1999), Experimental study of the ringing response of a vertical cylinder in breaking wave groups, *Int. J. Offshore and Polar Eng.*, Vol. 9, No. 4, pp. 276-282.

Werle B. (1995), Sea backscatter, spikes and wave group observations at low grazing angles, *IEEE Int. Radar Conf.*, pp. 187-195.

Wu M. (1997), Prediction of deck wetness and divergent bow waves on fine ships - nonlinear numerical studies, *PhD Dissertation*, UCSB, also OEL, Tech. Rpt. No. 97-150.

Yao Y.T, Wang P. and Tulin M.P. (1994), Wave-groups, wave-wave interactions and wave breaking, *Proc. 20th ONR Symp. on Naval Hydrodynamics*, Santa Barbara, Natl. Academy Press, pp. 551-567.

Yuen H.C and Lake B.M. (1982), Nonlinear dynamics of deep-water gravity waves, *Adv. Appl. Mech.*, Vol. 22, pp. 68-229.

Zakharov V.E. (1968), Stability of periodic waves of finite amplitude on the surface of deep fluid, *J. Appl. Mech. Tech. Phys.*, Vol. 2, pp. 190-194.

DISCUSSION

B. Beck
University of Michigan, USA

Looking at your figures, it appears that in the 2D+t computations, the diverging wave crest is a straight line. The figure using SPH in the cross flow plane seems to indicate the breaking wave front slows down so that the diverging wave crest is parabolic. Could you please comment on this?

AUTHOR'S REPLY

In Figures 30 and 31, the growing separation of the dipole vortical structure and the cresting breaker can be seen. The vortical structure is slower and would appear to follow a roughly parabolic track, although its asymptotic motion cannot yet be known from the limited calculations which we have done. The crest of the divergent wave is faster and its structure spreads with time. This corresponds physically to the growth in extent of the broken water just behind the crest and which would appear as a foam scar in the ocean. In front of this scar is the small surfing breaker. This marks the front of the broken wave. A line drawn through the center of the surfing eddies back to the touchdown of the original jet would appear to be reasonably straight. Again, further calculations in time must be made to understand the fate of the surfing eddy. It would seem reasonable to expect that it must eventually disappear.